Grasp and Manipulation Inspired by Human Motion

by

Tatsuya Shirai

Graduate School of Engineering,
Hiroshima University

March, 2001

Contents

List of Figures

List of Tables

Chapter 1

Introduction

1.1 Background

Robots are any kind of versatile mechanical device equipped with actuators and sensors under the control of a computing system. One of the ultimate goals in Robotics is to create autonomous robots. Such robots would accept high–level descriptions of tasks and execute them without further human intervention. The input descriptions would specify *what* the user wanted to do rather than *how* to do it. Our fascination with constructing mechanical analogues of ourselves has led us to place all sorts of hopes and expectations in robot capabilities. And yet it is a technology that is still in its infancy. It may be our own inability to appreciate the subtlety and power of the human mind and body that leads us to place such grand expectations in the future of robotics. Robots may indeed some day be super–human, but in the near future we should only expect more modest abilities. Making progress toward autonomous robots is of major practical interest in a wide variety of applications including manufacturing, construction, waste management, space exploration, undersea work, assistance for the disabled, and medical surgery. It is also of great technical interest, because it raises challenging and diverse issues from which new concepts of broad usefulness are likely

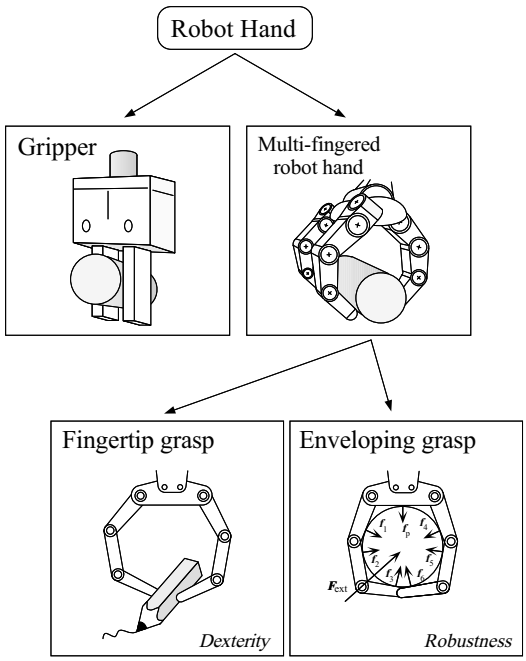

Fig. 1.1: Categorization of robot hands.

to emerge. It raises many important problems. One of them — the realization of dexterous robot hands — is the central theme of this dissertation.

The robot hand is an end–effector which is connected to the end of manipulator and used not only for grasping, but also for manipulating, the object to be grasped. Generally, robot hands can be categorized into the two types as shown in Fig.1.1. The gripper type hands are constructed of just one actuator and two fingers simply capable of opening and closing. They are implemented by most industrial robot, which can pick up an object moving on conveyer belt and place it in a designated area. Since the early 1980s, a number of grippers with various sensors, such as optical–range sensors, force sensors and slip–detection sensors have been designed and developed[1][2], allowing robots to achieve more sophisticated tasks. However, the gripper can not manipulate the object within its grasp, though it can change the grasping force by imparting an appropriate input for the actuator. On the other hand, multi–fingered

robot hands have the potential capability of manipulating an object dexterously, as human hands do. Therefore, by developing a dexterous multi–fingered robot hand, we can greatly extend the environment in which a robot can work. Based on this motivation, a number of projects for developing multi–fingered robot hands have been started in the early 1980s in various institutes. For example, Okada[3] has developed a three–fingered hand driven by a tendon and demonstrated the manipulation of a pencil by its fingertip. Salisbury[4] has designed and developed a three–fingered robot hand driven by four actuators per finger. The main contribution of this work was the reduction of the number of actuators by utilizing new power transmission mechanisms. The Utah/MIT hand[5] is one of the most sophisticated robot hands where each joint is driven by two pneumatic actuators specially designed for this project. These projects strongly stimulated the theoretical research on multi–fingered robot hands.

During 1980-1986, a number of papers discussing manipulation, sensing, control and kinematics have been published. These works implicitly assumed that fingertips were always in contact with the object to be manipulated and the inner links never touched it, as shown in Fig.1.1. In 1987, Salisbury first proposed the *Whole–Arm Manipulation (WAM)*[16, 17], where inner links were allowed contact with the object. Trinkle[23] has introduced the same idea to robot hands and gave us the term *Enveloping Grasp*. Such an enveloping grasp can support a large load in nature and is highly stable due to the large number of distributed contact points on the grasped object. Generally, in a fingertip grasp, we can expect dexterity in manipulation, while the robustness of grasp is its most advantageous feature for an enveloping grasp.

While both theory and hardware have been extremely advanced during the last two decades, we can not yet see the situation where multi–fingered robot hands work practically in various environments. Even though manipulation task is quite easy for humans,

robot hands often find it difficult to achieve. Why? What is the main reason? In order to find an answer to this question, this dissertation first executes a very simple grasp experiment by a human. By observing the human motion carefully, we discuss what makes it difficult for the robot hand to achieve exactly the same grasp motion and how we can implement motion planning into a robot so that it can achieve the same goal. We believe that the observation of humans will provide us with good hints for designing the motion planning of a robot hand.

1.2 Outline of this work

Now, suppose that cylindrical objects of various sizes, cross–section shapes, and surface friction, are placed on a table as shown in Fig.1.2. Actually, such a situation is often observed in a practical environment, for example, in grasping a table knife, an ice pick, a hammer, a wrench, and so on. In many cases, the tool handle can be modeled as a cylindrical shape. In chapter 2, we first observe the human motion for grasping column objects of different sizes, cross–section shapes and contact friction. Through this experiment, we newly found the *Scale–Dependent Grasp* where a human changes his (or her) grasping strategy depending on the size, friction, and geometry of objects. It should be noted that we do not intend to transfer exactly the same human motions to a robot hand just like a master–slave system shown in Fig.1.3 where the human motion detected by sensors is sent to the robot. The approach by a master–slave operation may succeed in grasping the object if the robot hand has the same degrees of freedom, configuration, number of fingers, and surface material as the human hand. Developed robot hands, however, have their own mechanical configurations and some are quite far from those of human hands. Under such conditions, the approach by the master–slave operation may easily fail to grasp an object. To cope with this, instead of fully

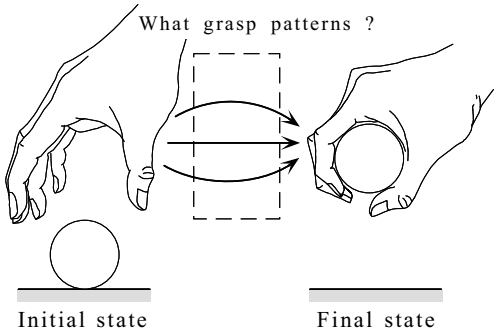

Fig. 1.2: Enveloping grasp for an object placed on a table.

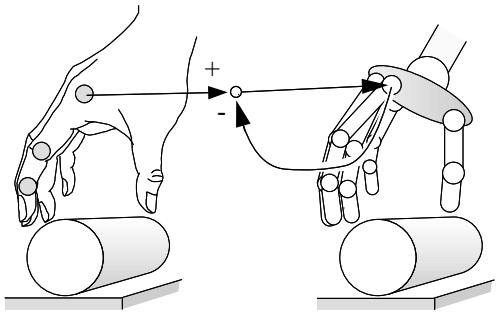

Fig. 1.3: Master–Slave System.

imitating human grasping, we extract the essential motions (or functions) from human behaviors so that we can easily apply them to a multi–fingered robot hand. Based upon such an interpretation of the human grasping motion, we discuss the grasping strategies applicable to a general multi–fingered robot hand. In choosing an appropriate strategy according to the size, friction and geometry of the object, we introduce a *guide–line–map*. We also include the discussion on how to choose an appropriate one among many strategies and how to switch from one to another when the robot hand fails to grasp the object.

In chapter 3, we focus on cylindrical objects whose diameters are relatively small. Through the observation of human grasping motion, we discovered an interesting behavior in which a human changes his finger posture from upright to crooked after all fingers have made contact with the object. This motion is termed the *detaching assist*

motion (DAM) and greatly contributes to achieving a detaching motion even for an object which is small enough to ensure that such a *wedge–effect* is not possible.

In chapter 4, we implement the *DAM* for the multi–fingered robot hand. We show that the *DAM* can be equivalently explained by the *Self–Posture Changing Motion (SPCM)*. As for the condition of lifting up the object, we explore a sufficient condition for always lifting up the object from a table utilizing the *SPCM*, and comparing this with contact stiffness model. We implement the *SPCM* in the grasping procedure of a three-fingered robot hand. Experimental results prove to be comparable with simulation results. Furthermore, we deal with the problem of estimating the stiffness of objects by utilizing active sensing.

In chapter 5, we confirm that the *DAM* effectively works for cylindrical objects of various sizes, shapes and contact friction. Based on experimental results, we propose a new grasp strategy, *Generalized Grasping Strategy (GGS)* where it includes the *DAM* in the central part. We experimentally show that a robot hand can achieve the enveloping grasp for a large range of objects by utilizing the *GGS*.

Finally, chapter 6 gives a summary of the dissertation.

1.3 Related work

Human grasping based approach: In robotic hands, there have been a number of papers learnt by human behaviors[6]–[12]. Cutkosky[6] has analyzed manufacturing grips and correlation with the design of robotic hands by examining grasps used by humans working with tools and metal parts. Bekey et al.[7] have presented the automatic grasp planner which generates an order set of grasp according to task description, heuristics, and geometry of an object. Kang and Ikeuchi[8][9] have proposed the *con-*

tact web and the *grasp cohesive index* for automatic classification of human grasping. Saito and Nagata[10] have proposed a method to classify and describe grasping and manipulation. It is based on three functions of grasping surfaces and provides simple description for grasping and manipulation. Kamakura[11] has classified the relationship between the purpose of task and the finger shape of human hand from the point of view of an occupational therapist. Shimizu et al.[12] have developed the sensor glove *MK III* that can measure the grasping force and its distribution. However, the grasping taxonomy proposed in these works have focused on either the final grasp mode or finding an appropriate grasp posture, while our work focuses on the whole grasping procedure for size of objects.

Approach phase: Jeannerod[13] has shown that during the approaching phase of grasping, human hand preshapes in order to prepare the shape matching with the object to be grasped. Bard and Troccaz[14] introduced such a preshaping motion into a robotic hand and proposed a system for preshaping a planar two–fingered hand by utilizing low–level visual data. Kaneko and Honkawa[15] have proposed a method for detecting a local contact point between a robot hand and an object by utilizing the *self–posture changing motion* where a finger link system with compliant joints can change its posture while making contact with an object.

Enveloping grasp (or power grasp): Salisbury et al.[16, 17] have proposed the *Whole–Arm Manipulation (WAM)* capable of treating a big and heavy object by using one arm allowing multiple contacts with an object. Mirza and Orin[18] have applied a linear programming approach to solve the force distribution problem in power grasps, and showed that the maximum weight of object which a robot hand can grasp increases significantly when the completely enveloping type of power grasp is utilized. Hirose

et al.[19] have proposed the *soft gripper* which can always produce constant torque in each joint simultaneously by using only two actuators. Bicchi[20] has showed that internal forces in power grasps can be decomposed into active and passive. Omata and Nagata[21] have analyzed the indeterminate grasp force by considering that sliding directions are constrained in power grasps. Zhang et al.[22] have evaluated the robustness of power grasp by utilizing the virtual work rated for all directions of virtual displacements.

Enveloping style manipulation: Trinkle, Abel and Paul[23] have analyzed planning techniques for enveloping without friction. Trinkle and Paul[24, 25] have proposed the *Initial Grasp Liftability Chart* (IGLIC) to analyze liftable condition for a frictionless object by using several pushers. Trinkle et al.[26] have discussed the quasistatic, "whole-arm," dexterous manipulation of enveloped slippery workpieces. They have considered grasp planning only under the assumption of low friction, while contact friction generally plays an important role to determine the grasp planning. Under constant torque control, Kaneko, Higashimori and Tsuji[27] have discussed the transition stability ensuring that the object moves stably from a table to the palm. They have proposed the *force–flow diagram* showing the accelerated direction at the point where the object is grasped. Kleinmann et al.[28] have showed a couple of approaches for finally achieving the power grasp from the fingertip grasp.

There have been a number of papers discussing fingertip based manipulation, where we can expect dexterous manipulation by using many degrees of freedom existing in the system. For example, Sarkar, Yun and Kumar[29], Cherif and Gupta[30], Kao and Cutkosky[31], Cole, Hsu and Sastry[32] discussed the rolling based manipulation and the sliding based manipulation. Also, there have been a couple of research

groups where they focused on non–prehensile manipulation. For example, pushing manipulation[33], graspless manipulation[34], orientation of planar polygonal parts[35] and toppling manipulation[36].

While there have been many works concerning the grasp, there is no work discussing the grasping strategy based on the *scale–effect* of objects.

1.4 Assumptions

We put several assumptions concerning the robot hands and the objects.

(A1-1) Robot hand is attached to the end of an arm. The hand position is measurable.

(A1-2) Robot hand includes a joint torque sensor, a joint angular sensor and a tactile sensor in the palm.

(A1-3) Each joint of robot hand can produce enough torque to manipulate an object.

(A1-4) Robot hand have n fingers and m_i links for the i-th finger.

(A1-5) Size of the objects is smaller than the size where the robot hand can cover more than the half of the circumference, and greater than the size where the robot hand can pick up or achieve a rotating motion on a table.

(A1-6) Objects are placed within the reachable area of robot hand.

(A1-7) Object is stiff enough.

1.5 Nomenclature

(Coordinate system)

Σ_R	Coordinate system fixed at the base.
Σ_B (Σ_{Fi})	Coordinate system fixed at the center of gravity of object (at i-th finger link).

(Superscript)

t	Transpose of matrix.
$\#$	Seudo–inverse matrix.
-1	Inverse matrix.
$\hat{}$	Value when contact force is projected on the friction boundary.
$*$	Value when the hand and the object have reached equilibrium.

(Subscript)

0	Value at initial posture ($0[sec]$).

(Symbol)

$\|\| \cdot \|\|$	Norm.
$diag$	Diagonal matrix.

(Variables)

$\boldsymbol{A}_k$	Coefficient matrix. $\boldsymbol{A}_k \in R^{3r \times 9}$.
$C_{\theta i}$	Compliance of s_i-th joint of i-th finger.
$\boldsymbol{c}_z$	Unit vector indicating the direction of z-axis in Σ_R. $\boldsymbol{c}_z = [0, 0, 1]^t$.

d_h	Normalized object size for human hand. $d_h = L_o/L_h$.
d_{link}	Half of the link width.
d_{obj}	Normalized object height. $d_{obj} = H_{object}/D_{tip}$.
d_{robot}	Normalized object size for robot hand. $d_{robot} = L_o/L_r$.
$\boldsymbol{D}$	$\boldsymbol{D} = \boldsymbol{S}^*\boldsymbol{N} \in R^{n\times(L-1)n}$.
D_{tip}	Diameter of fingertips of robot hand.
$\boldsymbol{e}_{ci}$	Unit vector which changes the orientation of $\boldsymbol{f}_{ci}$ into the nearest friction boundary.
$\boldsymbol{e}_i^k$	Factor of selection matrix $\boldsymbol{S}$. $\boldsymbol{e}_i^1 = [1, 0, ..., 0]^t \in R^{L\times 1}$ when $\boldsymbol{f}_{ci}$ exists on span vector $\boldsymbol{v}_i^1$.
$\boldsymbol{E}$	$\boldsymbol{E} = [\boldsymbol{I}_3, ..., \boldsymbol{I}_3] \in R^{3\times 3n}$.
$\boldsymbol{f}_{bias}$	Initial contact force vector. $\boldsymbol{f}_{bias} = \boldsymbol{K}_P\boldsymbol{J}\boldsymbol{K}_{\theta e}^{-1}\boldsymbol{\tau}_{bias}$.
$\boldsymbol{f}_{ci}$, $\boldsymbol{f}_c$	$\boldsymbol{f}_{ci}$ is the contact force vector at *i-th* contact point. $\boldsymbol{f}_c = [\boldsymbol{f}_{c1}^t, \ldots, \boldsymbol{f}_{cn}^t]^t \in R^{3n\times 1}$.
f_{ez}, f_{ezL}	Virtual force in the gravitational direction at the center of gravity of object. f_{ezL} is an upper limit of f_{ez}.
$\boldsymbol{f}_o$	Total force of the center of gravity of object. $\boldsymbol{f}_o \in R^{3\times 1}$.
$\boldsymbol{f}_{ti}$	$\boldsymbol{f}_{ti} = \boldsymbol{f}_{ci} - (\boldsymbol{n}_{CFi}^t\boldsymbol{f}_{ci})\boldsymbol{n}_{CFi}$.
$\boldsymbol{F}_{ci}$	$\boldsymbol{F}_{ci} = [\Delta f_{cix}^{(1)}, \Delta f_{ciy}^{(1)}, \Delta f_{ciz}^{(1)}, \ldots, \Delta f_{ciz}^{(r)}]^t$.
$\boldsymbol{g}$, g	Gravitational acceleration vector. $g = \|\|\boldsymbol{g}\|\|$
$\boldsymbol{G}$	Grasp matrix. $\boldsymbol{G} \in R^{3n\times 6}$.

$\boldsymbol{H}$

$$\boldsymbol{H} = \begin{bmatrix} \boldsymbol{J}_1^t \boldsymbol{V}_1 & & \mathbf{o} \\ & \ddots & \\ \mathbf{o} & & \boldsymbol{J}_n^t \boldsymbol{V}_n \end{bmatrix} \in R^{n \times Ln}.$$

H_{object} Height of object.

$\boldsymbol{I}$ Identical matrix. For example, $\boldsymbol{I}_3 = diag[1,1,1] \in R^{3\times 3}$.

I_a Maximum value among I_{a1} through I_{an}.

I_b Normalized distance between the palm and the representative position of object.

I_{ai} Normalized distance between each link surface of i-th finger and the object surface.

I_{ae} (I_{be}) Threshold for I_a (I_b).

I_{a_max} (I_{b_max}) Largest value of I_a (I_b) for all possible $\boldsymbol{p}_B$ in $\mathcal{V}_{pB}$.

$\boldsymbol{J}_i^t$ $(\boldsymbol{J}^t)$ Jacobian matrix mapping from $\boldsymbol{f}_{ci}$ $(\boldsymbol{f}_c)$ to τ_{si} $(\boldsymbol{\tau}_s)$.
$\boldsymbol{J}^t = diag[\boldsymbol{J}_1^t, \ldots, \boldsymbol{J}_n^t] \in R^{n\times 3n}$.

$\boldsymbol{K}_{Pi}$, $\boldsymbol{K}_P$ $\boldsymbol{K}_{Pi}$ is the contact stiffness matrix at i-th contact point between finger link and object.

$$\boldsymbol{K}_{Pi} = \begin{bmatrix} k_{ixx} & k_{ixy} & k_{ixz} \\ k_{iyx} & k_{iyy} & k_{iyz} \\ k_{izx} & k_{izy} & k_{izz} \end{bmatrix} \in R^{3\times 3}.$$

$\boldsymbol{K}_P = diag[\boldsymbol{K}_{P1}, \ldots, \boldsymbol{K}_{Pn}] \in R^{3n\times 3n}$.

$\boldsymbol{K}_{Psi}$ $\boldsymbol{K}_{Psi} = [k_{ixx}, k_{ixy}, k_{ixz}, \ldots, k_{izx}, k_{izy}, k_{izz}]^t$

$\boldsymbol{K}_{Pe}$ Stiffness matrix with respect to $\boldsymbol{P}_{CBi}$ on the surface of object.
$\boldsymbol{K}_{Pe} = \boldsymbol{K}_P\{\boldsymbol{I} - \boldsymbol{J}(\boldsymbol{K}_\theta + \boldsymbol{J}^t\boldsymbol{K}_P\boldsymbol{J})^{-1}\boldsymbol{J}^t\boldsymbol{K}_P\}$.

$\boldsymbol{K}_\theta$ Stiffness matrix of compliant controlled joints.
$\boldsymbol{K}_\theta = diag[k_{\theta 1}, \ldots, k_{\theta n}] \in R^{n\times n}$ where $k_{\theta i} = 1/C_{\theta i}$.

$\boldsymbol{K}_{\theta e}$ Combined stiffness matrix which is composed of both the stiffness $\boldsymbol{K}_\theta$ and the joint stiffness $\boldsymbol{J}^t\boldsymbol{K}_P\boldsymbol{J}$.
$\boldsymbol{K}_{\theta e} = \boldsymbol{K}_\theta + \boldsymbol{J}^t\boldsymbol{K}_P\boldsymbol{J}$.

l_1, l_2, l_3	Length of each link. The robot hand used in the experiments : $l_1 = 40[mm]$, $l_2 = 25[mm]$, $l_3 = 25[mm]$.
L_{aij}	Length between the surface of link j of i-th finger and geometrical center of object $\boldsymbol{p}_B$.
L_b, L_{b_max}	Distance between the palm and geometrical center of object $\boldsymbol{p}_B$. L_{b_max} is a largest value in $\mathcal{V}_{pB}$.
L_{gap}	Distance between fingertips of robot hand. $L_{gap} = 0$ when each finger link has an intersection.
L_h	Length from the tip of thumb to the tip of index finger for human hand.
L_o	Length of the circumference of object.
L_r	Length between fingertips of robot hand. L_r corresponds to the parameter L_h for human hand.
m_i	Number of joint of i-th finger.
m_B	Mass of object.
n	Number of finger.
$\boldsymbol{N}$	Full rank matrix satisfying $\boldsymbol{H}\boldsymbol{N} = \mathbf{o}$. $\boldsymbol{N} \in R^{Ln \times (L-1)n}$.
$\boldsymbol{n}_{btm}$	Unit normal vector directing inside at contact point on the bottom part of object.
$\boldsymbol{n}_{CBi}$ $(\boldsymbol{n}_{CFi})$	Unit normal vector directing outside at i-th contact point on the surface of object (i-th finger).
$\boldsymbol{n}_{CFij}$	Unit normal vector directing outside at j-th contact point on the surface of i-th finger.
$\boldsymbol{p}_B$ $(\boldsymbol{p}_{Fi})$	Position vector of Σ_B (Σ_{Fi}) with respect to Σ_R. $\boldsymbol{p}_B = [p_{Bx}, p_{By}, p_{Bz}]^t$.
$\boldsymbol{p}_{Ci}$	Position vector of i-th contact point with respect to Σ_R.
${}^B\boldsymbol{p}_{CBi}$ $({}^{Fi}\boldsymbol{p}_{CFi})$	Position vector of i-th contact point with respect to Σ_B (Σ_{Fi}).

$\boldsymbol{p}_{top}$, $\boldsymbol{p}'_{top}$	Pushing point for rotating an object on a table. Pushing point when $\boldsymbol{p}_{top}$ can not be detected on an object.
r	Number of push–in motion for detecting the contact stiffness of object.
$\boldsymbol{R}_B$ ($\boldsymbol{R}_{Fi}$)	Rotation matrix of Σ_B (Σ_{Fi}) with respect to Σ_R.
$\boldsymbol{S}$, $\boldsymbol{S}^*$	Selection matrix. $\boldsymbol{S} = diag[\boldsymbol{e}^t_{1k}, ..., \boldsymbol{e}^t_{nk}] \in R^{n \times nL}$. $\boldsymbol{S}^* = diag[\boldsymbol{\Gamma}_1, ..., \boldsymbol{\Gamma}_n] \in R^{n(L-1) \times nL}$.
$S_B({}^B\boldsymbol{p})$ $(S_{Fi}({}^{Fi}\boldsymbol{p}))$	Function representing the surface shape of object (i-th finger link).
T_a	Timing which an object suddenly start to move up with rotating motion on human observation of *DAM*.
$\boldsymbol{u}$	Arbitrary vector. $\boldsymbol{u} \in R^{Ln \times 1}$.
$\boldsymbol{U}_i$, $\boldsymbol{U}$	Linear transformation matrix. $\boldsymbol{U}_i \in R^{3 \times 3}$. $\boldsymbol{U} = diag[\boldsymbol{U}_1, \ldots, \boldsymbol{U}_n] \in R^{3n \times 3n}$.
$\boldsymbol{v}^k_i$	k-th span vector of L-faced polyhedral convex at i-th contact point.
$\boldsymbol{V}_i$	Span vector matrix of L-faced polyhedral convex at i-th contact point. $\boldsymbol{V}_i = [\boldsymbol{v}^1_i, \ldots, \boldsymbol{v}^L_i] \in R^{3 \times L}$.
$\mathcal{V}_{pB}$	Area of the candidate of $\boldsymbol{p}_B$.
$\boldsymbol{W}_{ext}$	Load wrench. $\boldsymbol{W}_{ext} \in R^{6 \times 1}$.
W_f, W_t	Width at the bottom and width at a bit higher position of object.
$\boldsymbol{w}_i$	Arbitrary vector. $\boldsymbol{w}_i \in R^{3 \times 1}$.
α	Friction angle between a object and a link.
β_1, β_2	Angle between an edge of the object and the table.
$\boldsymbol{\Gamma}_i$	$\boldsymbol{\Gamma}_i = [\boldsymbol{e}^1_i, ..., \boldsymbol{e}^{(k-1)}_i, \boldsymbol{e}^{(k+1)}_i, ..., \boldsymbol{e}^L_i]^t \in R^{(L-1) \times L}$.
Δp_{By}	$\Delta p_{By} = p_{By} - p_{By0}$.
$\Delta\theta_B$	$\Delta\theta_B = \theta_B - \theta_{B0}$.
$\Delta\theta_{ia}$, $\Delta\theta_{ta}$	$\Delta\theta_{ia} = \theta_{ia} - \theta_{ia0}$, $\Delta\theta_{ta} = \theta_{ta} - \theta_{ta0}$.

$\Delta\theta_{ik}$, $\Delta\theta_{tk}$ $\Delta\theta_{ik} = \theta_{ik} - \theta_{ik0} \mid_{k=1,2,3}$. $\Delta\theta_{tk} = \theta_{tk} - \theta_{tk0} \mid_{k=1,2}$.

$\Delta\theta_{pi}$ Angular displacement for p_i-th joint of i-th finger ($i = 1, \ldots, n$).

$\Delta\boldsymbol{\theta}_p$ Angular displacement matrix of position controlled joints.
$\Delta\boldsymbol{\theta}_p = [\Delta\theta_{p1}, \ldots, \Delta\theta_{pn}]^t \in R^{n\times 1}$.

$\Delta\theta_{si}$ Angular displacement for s_i-th joint of i-th finger ($i = 1, \ldots, n$).

$\Delta\boldsymbol{\theta}_s$ Angular displacement matrix of compliant controlled joints.
$\Delta\boldsymbol{\theta}_s = [\Delta\theta_{s1}, \ldots, \Delta\theta_{sn}]^t \in R^{n\times 1}$.

$\boldsymbol{\theta}_i$ Joint angle vector for i-th finger of robot hand.
$\boldsymbol{\theta}_i = [\theta_{i1}, \theta_{i2}, \ldots, \theta_{im}]^t$.

θ_{btm} Angle between the horizontal line and the normal vector $\boldsymbol{n}_{btm}$ at the contact point.

θ_{ia}, θ_{ta} Absolute angle of tip of index finger and thumb.

θ_{i1}, θ_{i2}, θ_{i3} Relative angle at each joint of index finger (positive for CCW).

θ_{t1}, θ_{t2} Relative angle at each joint of thumb (positive for CW).

θ_B Rotating angle of object (positive for CCW).

λ_i^k, $\boldsymbol{\lambda}_i$, $\boldsymbol{\lambda}$ Scalar of $\boldsymbol{f}_{ci}$ which exists on the k-th span of polyhedral convex.
$\boldsymbol{\lambda}_i = [\lambda_i^1, ..., \lambda_i^L]^t \in R^{L\times 1}$.
$\boldsymbol{\lambda} = [\boldsymbol{\lambda}_i^t, ..., \boldsymbol{\lambda}_n^t]^t \in R^{Ln\times 1}$.

μ Friction coefficient between a object and a link.
$\mu = \tan\alpha$

$\boldsymbol{\tau}_{bias}$ Torque vector of initial torque at compliant joints.
$\boldsymbol{\tau}_{bias} = -\boldsymbol{K}_\theta \Delta\boldsymbol{\theta}_s \in R^{n\times 1}$.

$\boldsymbol{\tau}_i$ Torque vector of i-th finger.
$\boldsymbol{\tau}_i = [\tau_{i1}, \tau_{i2}, \ldots, \tau_{im}]^t$.

$\boldsymbol{\tau}_s$ Torque vector at compliant joints. $\boldsymbol{\tau}_s = [\tau_{s1}, \ldots \tau_{sn}]^t \in R^{n\times 1}$.

$\boldsymbol{\Phi}$ Arbitrary vector. $\boldsymbol{\Phi} \in R^{(L-1)n\times 1}$

(Contact stiffness model)

$\delta\boldsymbol{P}_i$, $\delta\boldsymbol{P}$ Position vector from $\boldsymbol{p}_{CFi}$ to $\boldsymbol{p}_{CBi}$. $\delta\boldsymbol{P}_i \in R^{3\times 1}$.
Position vector matrix. $\delta\boldsymbol{P} = [\delta\boldsymbol{P}_1^t, \ldots, \delta\boldsymbol{P}_n^t]^t \in R^{3n\times 1}$.

$\delta \boldsymbol{x}$	Vector expressing the displacement and rotation of object. $\delta \boldsymbol{x} \in R^{6\times 1}$
$\delta \boldsymbol{\theta}_s$	Vector expressing the angular displacement of compliant joints. $\delta \boldsymbol{\theta}_s \in R^{n\times 1}$

Chapter 2

Scale–Dependent Grasp

2.1 Introduction

In order to observe human behaviors, we asked a subject to achieve the enveloping grasp for an object placed on a table. We are interesting to know how human approaches and grasps the object. Moreover, we are also interesting to observe how human changes his (or her) grasp strategy according to the size of objects to be grasped. We will also discuss that when implementing the grasp strategy to a robot hand, what is the major barriers and how we can overcome.

2.2 Human Observation

2.2.1 Introduction of Non–Dimensional Object's Size

Fig.2.1 shows the objects used in our experiments, where the white and the black surfaces denote that they are covered by a drawing paper and a rubber, respectively, so that we can purposely change the contact friction. Now, suppose two subjects, where they have a big hand and a small hand, respectively. Also, suppose that each

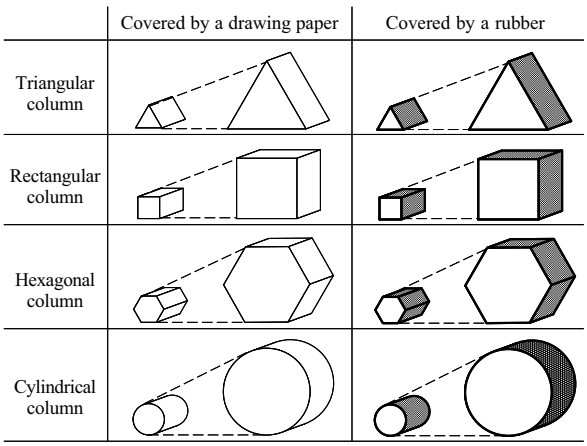

Fig. 2.1: Column objects used in the experiments.

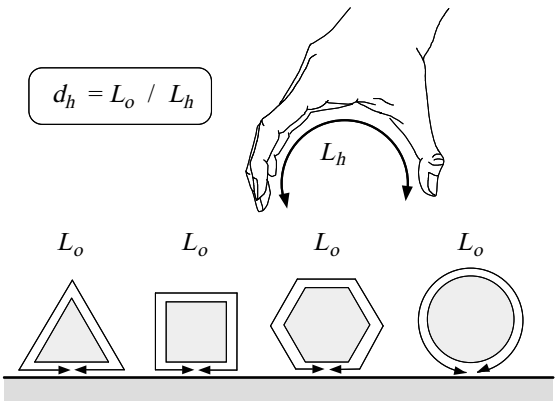

Fig. 2.2: Explanation of L_o and L_h.

subject approaches and grasps the same object. In such a case, the subject with a big hand should feel the object relatively smaller than the subject with a small hand feels. To avoid such *scale–effect* depending on the size of object, we introduce the normalized object size d_h defined by $d_h = L_o/L_h$, where L_h and L_o denote the length from the tip of thumb to the tip of index finger, and the length of the circumference of object, respectively, as shown in Fig.2.2. For experiments, we prepared six kinds of objects whose sizes are $2.80 \geq d_h \geq 0.26$.

2.2.2 Grasp Pattern Classification

Fig.2.3 shows the experimental results for column objects, where "No." denotes the number of subjects taking the particular grasp pattern, and the cross–section shape of object is illustrated in the bottom of each figure. Each grasp pattern is explained in the following.

Pattern–1 (*Direct grasp*) : Without any re-grasping motion, human directly grasps the object (Fig.2.4(a)).

Pattern–2 (*Sliding based grasp*) : This pattern utilizes the sliding motion between the finger link and the object. fingertips push the part between the bottom of object and the table, such that the object can be lifted up (Fig.2.4(b)). This is what we call the *wedge–effect* where an object receives quite a big lifting force produced by fingertips inserted into narrow gap between the table and the object.

Pattern–3 (*Rolling based grasp*) : The object is rolled up over the surface of thumb (or index finger). After the object is lifted up from the table, each finger link is closed to achieve the enveloping grasp (Fig.2.4(c)).

Pattern–4 (*Regrasping based grasp*) : The object is first picked up by thumb and index (or middle) fingertips. The remaining fingers hook the object and then squeeze it till the fingertip grasping is broken. Finally, the object comes in contact with the palm (Fig.2.4(d)).

For a large object ($1.0 \leq d_h < 2.8$), human directly grasps it (*pattern–1*), irrespective of the cross–section shape and the contact friction. As the size of object decreases ($0.5 \leq d_h < 1.0$), pattern–2 through 4 appear according to the personal choice as well

as the conditions set for the experiment. For this size of object, some subjects take the *sliding based grasp* (*pattern–2*), when the surface friction is small. On the other hand, for the object with significant friction, *sliding based grasp* (*pattern–2*) disappears and, instead, both *rolling based grasp* (*pattern–3*) and *regrasping based grasp* (*pattern–4*) become dominant. The change of grasp patterns is naturally understandable, because it is hard to achieve a sliding motion under a significant friction while both rolling and regrasping motions can be realized irrespective of the contact friction. Pattern–4 especially becomes dominant for a small object ($0.26 \leq d_h < 0.5$). For such a small object, human tries to avoid interference between the fingertip and the table. As a result, human first picks up the object and achieves the target grasp through regrasping process from the fingertip to the enveloping grasps.

Through the experimental results, we make clear that human chooses a grasp planning according to the size of object, even though they are geometrically similar. We call the grasp planning the *scale–dependent grasp* planning. We would note that the *scale–dependent grasp* does not mean the final grasp style but means the change of grasp patterns observed between the initial and the final states according to the size of objects.

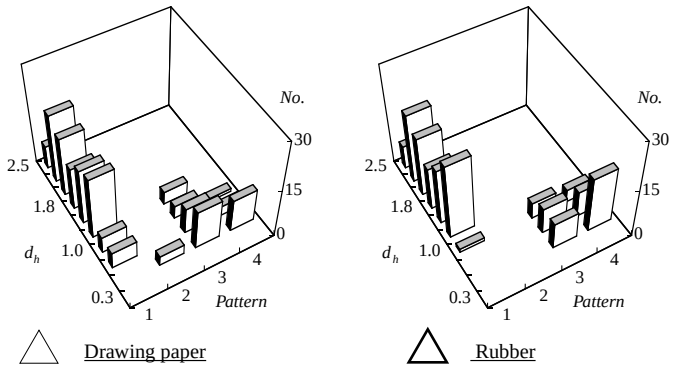

(a) Triangular column

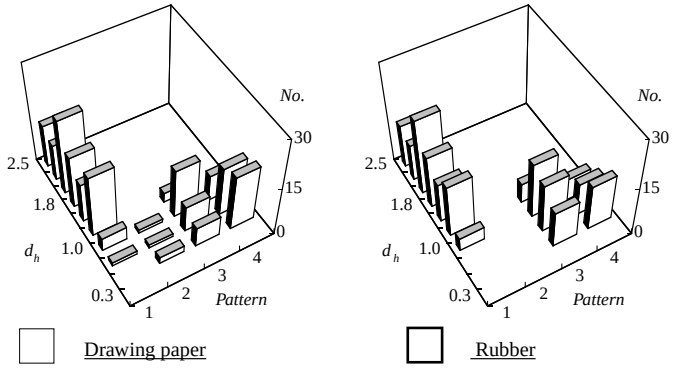

(b) Rectangular column

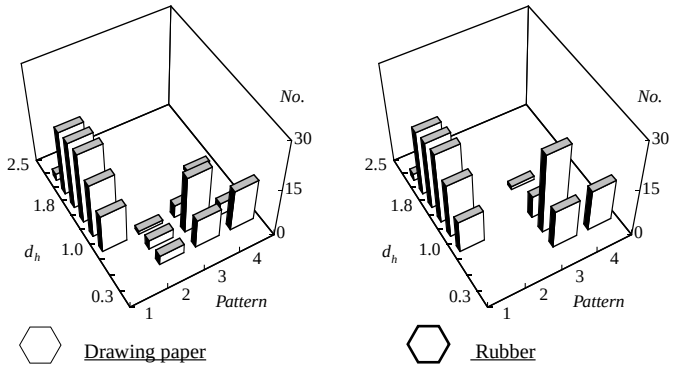

(c) Hexagonal column

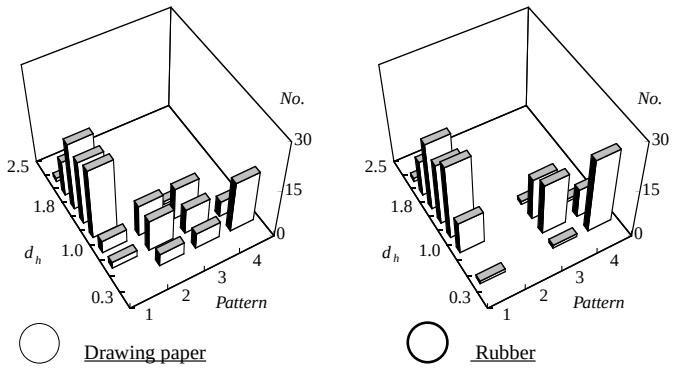

(d) Cylindrical column

Fig. 2.3: Grasp pattern classification map.

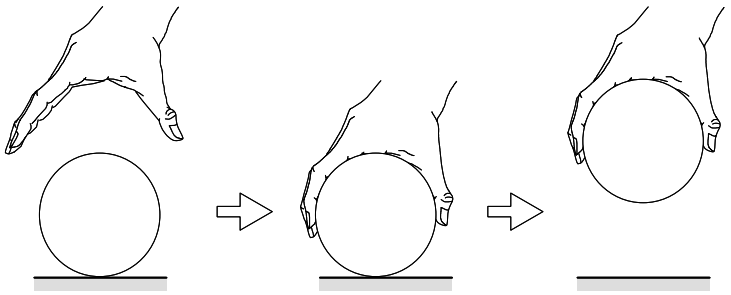

(a) Pattern-1 (Direct Grasp)

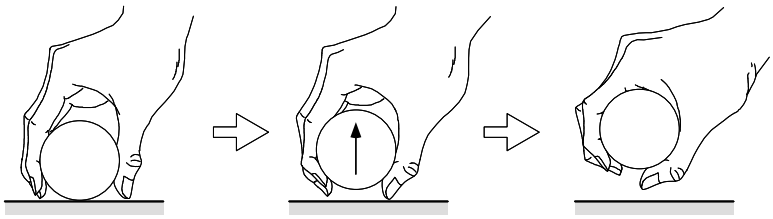

(b) Pattern-2 (Sliding based Grasp)

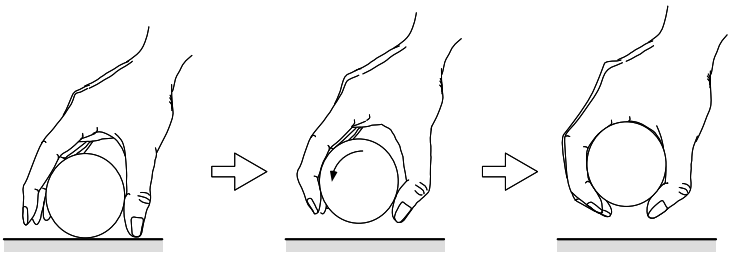

(c) Pattern-3 (Rolling based Grasp)

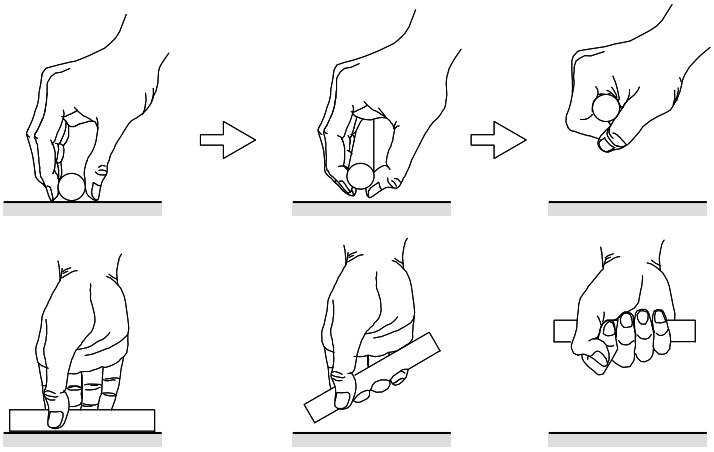

(d) Pattern-4 (Regrasping based Grasp)

Fig. 2.4: Grasp patterns.

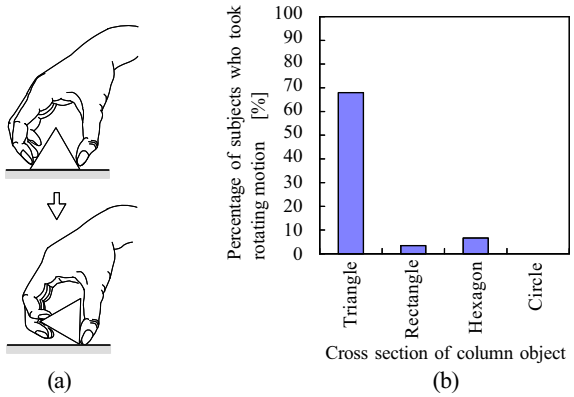

Fig. 2.5: Initial adjustment motion

2.2.3 Initial Adjustment Motion

An interesting behavior is observed at the initial phase in grasping triangular objects. Almost 70% of subjects first rotate the object around an edge so that a couple of fingers can be inserted in the gap between the object and the table as shown in Fig.2.5 , where Fig.2.5(a) explains the basic motion at the initial phase and Fig.2.5(b) shows percentage of subjects utilizing the rotating motion. For grasping a triangular object, such a rotating motion is indispensable for detaching the object from the table. We call this motion the *initial adjustment motion*. We note that the *initial adjustment motion* dominantly appears only for triangular objects.

2.2.4 Interpretation of Grasping Motions

Human grasping provides good hints for constructing grasping strategies of a robot hand. However, as mentioned in section 1.2, transferring the exact grasping motion to a robot hand may often fail in grasping an object, since each robot hand has its own mechanical configuration and structure as shown in Fig.2.6. In this subsection, we provide an interpretation of human grasping, so that we can construct grasping strategies easily applicable to multi–fingered robot hands. For achieving an enveloping

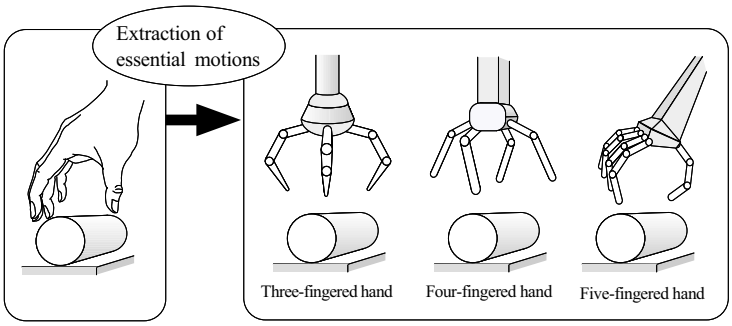

Fig. 2.6: Interpretation of human grasping.

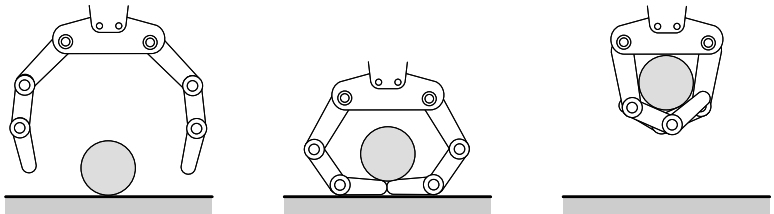

Fig. 2.7: Intermediate phase

grasp by a robot hand, surrounding an object by robot fingers as shown in Fig.2.7(b) will provide us with a good starting point for a next step. For example, the transition from Fig.2.7(b) to Fig.2.7(c) will be realized by simply closing each finger joint. Based on this consideration, we set an intermediate phase between the initial and the goal states as shown in Fig.2.7 and roughly separate the grasping procedure into the following three tasks.

Task 1 : Detaching the object from a table and capturing it within the hand.

Task 2 : Lifting up the object.

Task 3 : Grasping the object firmly.

Detaching the object from a table is the starting motion for further steps. For example, detaching can be achieved by utilizing the *wedge–effect* or *picking up motion* or *rolling motion*. Lifting up can be achieved by *sliding motion* or *rolling motion*.

2.3 Robot Application

For our convenience, we first define several parameters for robot hands as shown in Fig.2.8. We utilize the normalized length d_{robot} defined by $d_{robot} = L_o/L_r$, where L_o and L_r denote the circumference of the object and the length between fingertips, respectively. L_r corresponds to the parameter L_h for human hand. The parameter H_{object} is the height of object, and the corresponding diameter for fingertip is defined by D_{tip}. $\boldsymbol{p}_B$, $\boldsymbol{n}_{CFij}$, L_{aij} and L_b are the geometrical center of object, a unit normal vector perpendicular to the surface of link j of i-th finger, and the length between the surface of link j of i-th finger and $\boldsymbol{p}_B$, and the distance between the palm and $\boldsymbol{p}_B$, respectively. L_{gap} is defined by the distance between fingertips, where we set $L_{gap} = 0$ when each finger link has an intersection. With both assumptions (A1–1) and (A1–2), the robot hand can obtain H_{object}, while it can be obtained more easily if it has a vision sensor.

In addition, we put two assumptions for simplicity :

(A2-1) Objects have column shape and their cross–section shapes are regular polygon where all sides of cross section and angles are equal.

(A2-2) Each finger motion is restricted to a planar motion.

2.3.1 Success Condition for Achieving an Enveloping Grasp

Before proceeding the precise discussion, we define the success condition for achieving an enveloping grasp in our work.

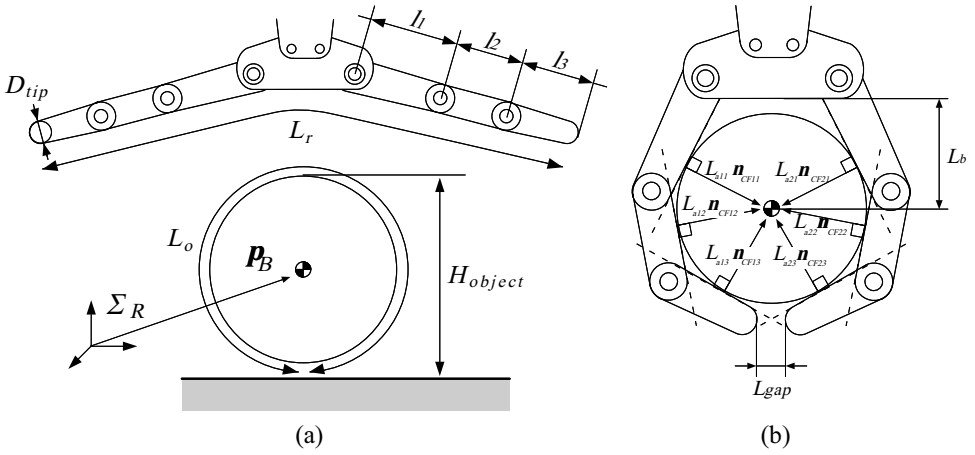

Fig. 2.8: The relationship between the robot hand and the object.

[Success condition of enveloping grasp]

It is defined that a robot hand completes an enveloping grasp for an object, if the following conditions are satisfied.

$$I_a \leq I_{ae} \quad \cap \quad I_b \leq I_{be} \quad \cap \quad L_{gap} < H_{object}, \tag{2.1}$$

where

$$I_a = max\{I_{ai} = \sum_{j=1}^{m_i} \frac{|(H_{object}/2) - L_{aij}|}{H_{object}}, i = 1, 2, ..., n\}, \tag{2.2}$$

$$I_b = \frac{L_b}{(H_{object}/2)}, \tag{2.3}$$

I_{ae} and I_{be} are thresholds for I_a and I_b, respectively. I_a is the maximum value among I_{a1} through I_{an}. I_{ai} represents the normalized distance between each link surface and the object surface, and I_b represents the normalized distance between the palm and the representative position of object.

For a cylindrical object, $I_a = 0$ and $I_b = 1$ if the object makes contact with all finger links and the palm. However, for a general column object, both $I_a = 0$ and $I_b = 1$ are not kept anymore, even if the robot hand fully envelops the object. To cope with this,

we have to choose the thresholds (I_{ae}, I_{be}) carefully.

For computing both I_a and I_b, we need to know $\boldsymbol{p}_B$. If the robot hand includes a vision sensor, it can directly obtain $\boldsymbol{p}_B$ from the image information. Even if this is not the case, the robot can judge the *success condition of enveloping grasp* by joint angular sensor to some extent. L_{gap} can be obtained by joint angular sensor only, while both I_a and I_b need $\boldsymbol{p}_B$ to compute L_{aij} and L_b. Suppose that cross–section shape is not given. Since the palm sensor is available by assumption A1–2, the robot hand can measure the object's height H_{object}. However, since the robot does not know the cross–section shape of object, the candidate of $\boldsymbol{p}_B$ generally forms an area $\mathcal{V}_{pB}$ as shown in Fig.2.9(b). To obtain $\mathcal{V}_{pB}$, we define the circle C whose diameter is equal to that of the inscribed circle of the cross–section. For example, Fig.2.9(a) shows the relationship between H_{object} and the diameter of C for a triangular object. Since the finger link never reaches the inside of C, we can obtain the candidate of $\boldsymbol{p}_B$ as shown in Fig.2.9(b). Now, we consider the worst scenario in a sense of having the largest area of $\mathcal{V}_{pB}$. The worst scenario is expected when we assume triangular cross–section, while we have the smallest area of $\mathcal{V}_{pB}$ for a cylindrical object. For all possible $\boldsymbol{p}_B$ in $\mathcal{V}_{pB}$, we obtain the largest I_{a_max} and I_{b_max}, so that we can evaluate the worst case. If I_{a_max} and I_{b_max} satisfy the following success condition, we say that the enveloping grasp is completed.

$$I_{a\_max} \leq I_{ae} \ \cap \ I_{b\_max} \leq I_{be} \ \cap \ L_{gap} < H_{object} \tag{2.4}$$

2.3.2 Experimental System

Fig.2.10(a) shows a structure of a robot hand used in the experiments where the robot hand consists of three same finger units and each finger has three links. The lengths of each link are $l_1 = 40[mm]$, $l_2 = 25[mm]$, and $l_3 = 25[mm]$, respectively. Each

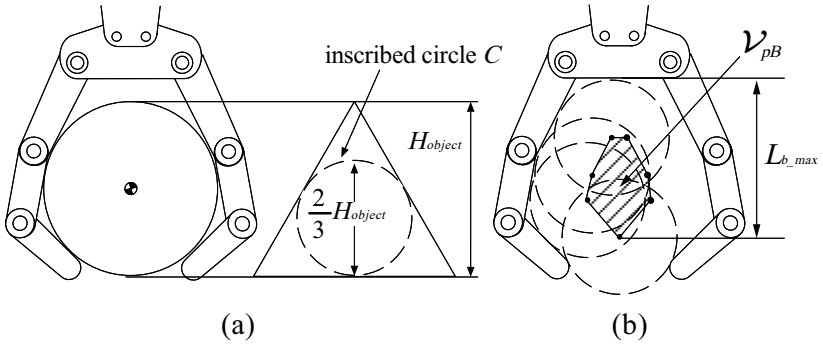

Fig. 2.9: Estimate that the area of $\boldsymbol{p}_B$.

finger link is driven by wire and a torque sensor is included in each joint. Rotary encoder is used as an angular sensor. The palm is equipped with ON/OFF type tactile sensor. Fig.2.10(b) shows an overview of the experimental system where the system is controlled by a 32-bit personal computer. The outputs from the torque sensors, the rotary encoders and the tactile sensor are fed into computer through an A/D converter board, a counter board and Digital I/O board, respectively. The DC servo motor is controlled by a servo driver where the control signal is sent through a D/A converter board. The table is controlled towards up and down by using one-axis slider.

2.3.3 Guide–Line–Map for Choosing an Appropriate Strategy

Fig.2.11 shows a *guide–line–map* for choosing an appropriate strategy according to the size, cross–section shape and contact friction of objects. Table 2.1 shows the names corresponding each group $A \sim D$ in Fig.2.11. Let α and θ_{btm} be an angle of friction and an angle between the horizontal line and the normal vector $\boldsymbol{n}_{btm}$ at the bottom part of object as shown in Fig.2.12, respectively. Fig.2.11(a) shows the *guide–line–map* under the condition that the contact friction between finger links and the object is small ($\alpha < \theta_{btm}$), where the horizontal and the vertical axes denote the nondimensional

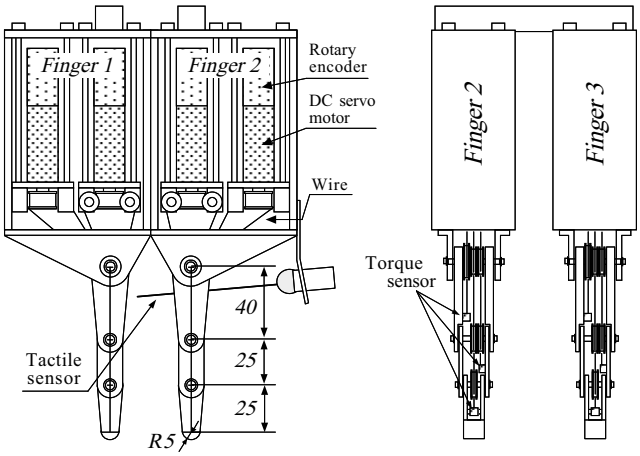

(a) Structure of a three-fingered robot hand

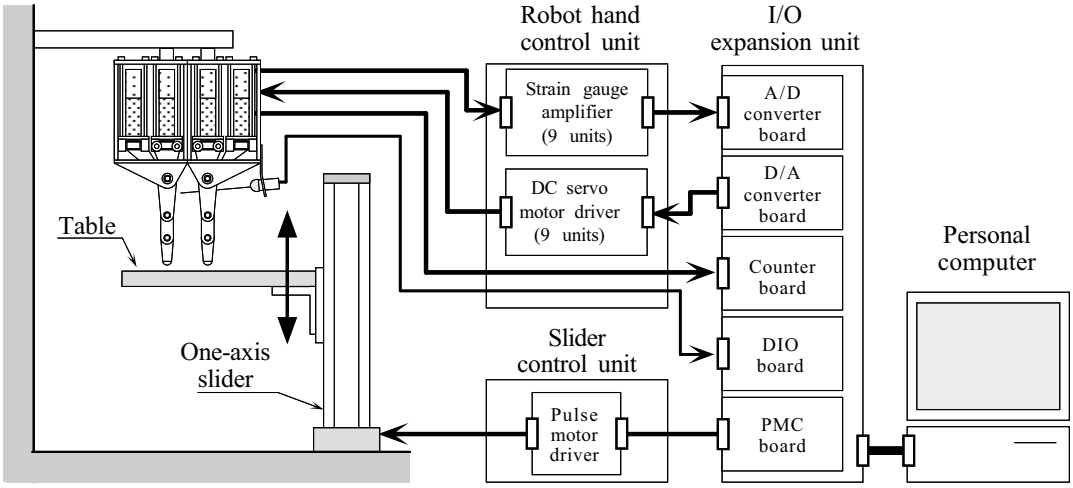

(b) Structure of experimental system

Fig. 2.10: Overview of robot hand system.

object size d_{robot} and the shape of object, respectively. On the other hand, Fig.2.11(b) shows the *guide–line–map* under the condition where the contact friction is significant ($\theta_{btm} \leq \alpha$).

Let us now discuss how to realize three tasks given in subsection 2.2.4. The simplest way for achieving Task 1 (Detaching the object) is to pick up an object by fingertips. However, if a robot hand regrasps an object from fingertip to an enveloping grasps in

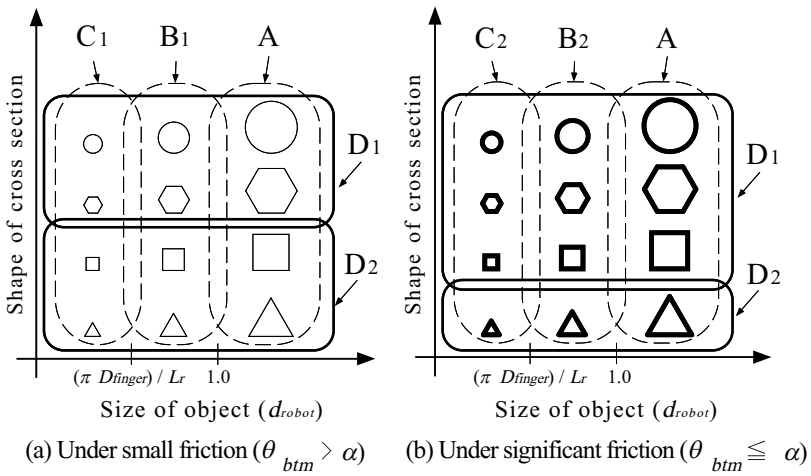

Fig. 2.11: The map for choosing an appropriate strategy for achieving enveloping grasp.

Table 2.1: Groups of grasping strategies

Group	*Grasping strategy*
A	Direct grasp
B_1	Sliding based grasp
B_2	Rolling based grasp
C_1	Regrasping based grasp
C_2	Regrasping based grasp with Rolling motion
D_1	Without Rotating motion
D_2	With Rotating motion

the open space in the air, it will often drop the object on the table. If the object is fragile, it will be broken. To avoid such an undesirable scenario, we make the grasp planning so that a part of object can make contact with the table as much as possible until the object is firmly grasped within the hand. Therefore, executing the detaching motion by a robot hand will differ from that of human. Task 2 (Lifting up the object) is achieved either by sliding or rolling motion, depending upon the contact friction over the object's surface as human does. We execute Task 3 (Grasping the object firmly) by constant torque control which is widely used in the research of power grasp [22, 27, 37]. The constant torque control can be achieved by adjusting actuator's current based on the torque sensor output. The control has an advantage where both finger posture

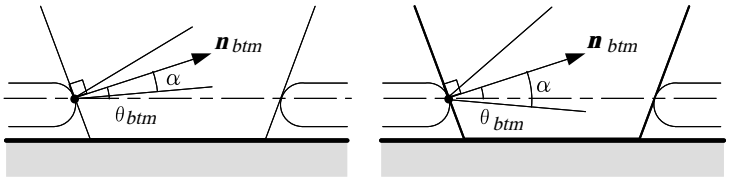

(a) $\alpha < \theta_{btm}$ (b) $\theta_{btm} \leqq \alpha$

Fig. 2.12: Two kinds of the contact frictions.

and contact force between the finger links and the object are determined automatically according to the command torque. While the grasping motions may differ from those of human and also vary depending upon the mechanical structure of robot hands, the basic tasks constructing the grasping strategy do not change irrespective of the hardware of robot hands. In the following sections, we explain how to realize each group for a robot hand.

2.3.4 Without Initial Adjustment Motion : Group–D_1

◯ **Group–A : Direct grasp** $(1.0 \leq d_{robot})$

For an object satisfying this condition, constant torque control is applied to each joint after the palm makes contact with the object, as shown in Fig.2.13(a). After an enveloping grasp is completed, the robot arm can move the object as shown in Fig.2.13(b). We note that it is not necessary for the hand to realize detaching and lifting motions, since they are achieved by the arm.

Task 1 (Detaching motion)	**: no need**
Task 2 (Lifting motion)	**: no need**
Task 3 (Grasping motion)	**: Constant torque command**

(a) Enveloping phase (b) Object transfer phase

Fig. 2.13: Direct grasp.

○ Group–$\mathbf{B}_1$: Sliding based grasp

$$((\pi D_{tip})/L_r \leq d_{robot} < 1.0 \ \cap \ \textit{Contact friction is small})$$

For an object satisfying this condition, the robot hand utilizes a sliding motion between the object and fingers for detaching the object from a table. Initially each finger is opened as shown in Fig.2.14(a) and then approaches the table until the fingertip makes contact with it, where the table detection can be easily checked by torque sensor outputs. In the next step, each fingertip follows along the surface of table until a part of finger link makes contact with the object as shown in Fig.2.14(b). This phase is what we call approach phase. The approach phase is inserted for every strategy except for the *direct grasp*, while we omit the explanation of approach phase in the following discussions. Then, each fingertip pushes the bottom part of object each other, so that we can make the most use of the *wedge–effect*. The object will be automatically lifted up by slipping over the finger surface as shown in Fig.2.14(c). At the same time, each link is gradually closed to fully constrain the object. In this strategy, constant torque control is also effectively utilized for achieving Task 1 through 3. Whether the object really reaches the palm or not strongly depends on how much torque command is imparted to each joint.

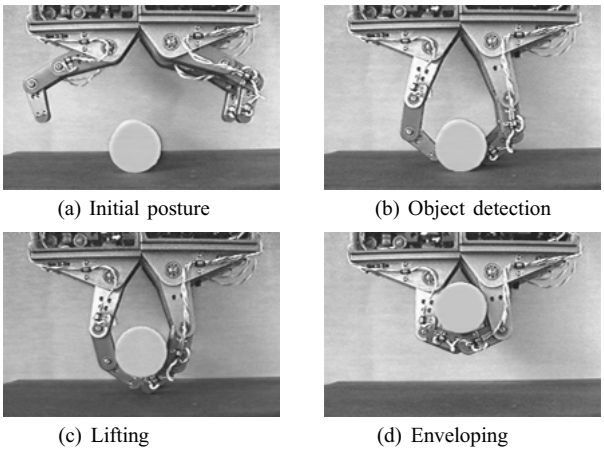

(a) Initial posture (b) Object detection

(c) Lifting (d) Enveloping

Fig. 2.14: Sliding based grasp.

Task 1 (Detaching motion)	**: Constant torque command**
Task 2 (Lifting motion)	**: Constant torque command**
Task 3 (Grasping motion)	**: Constant torque command**

Fig.2.15 shows the success classification map for a cylindrical object with $H_{object} = 32[mm]$ and $\mu = 0.7$, where the horizontal and the vertical axes denote the normalized command torque $\tau_1/(m_B g l_1)$, $\tau_2/(m_B g l_2)$ for the first and the second joints under $\tau_3/(m_B g l_3) = \tau_2/(m_B g l_2)$, respectively, and ◯ and the other three marks($\times$, ■, ♢) correspond to the final grasping postures as shown in the top of the graph. The judgment of success or failure is achieved by examining I_a and I_b which are also given in Fig.2.15. From Fig.2.15, we can see that a large area of torque commands is obtained for achieving the enveloping grasp under $\mu = 0.7$.

◯ **Group–B$_2$: Rolling based grasp**

$$((\pi D_{tip})/L_r \leq d_{robot} < 1.0 \ \cap \ \textit{Contact friction is large}\ )$$

Fig.2.16 shows the success classification map for a cylindrical object ($H_{object} = 32[mm]$) under $\mu = 1.3$. We note that the region(◯) where the hand envelops an object successfully, disappears under $\mu = 1.3$. This is because a sliding motion based on the

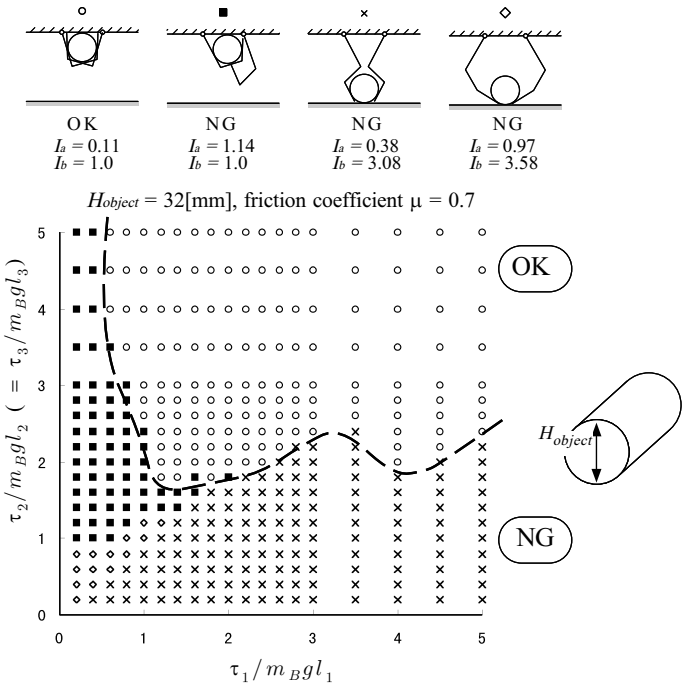

Fig. 2.15: Success map for a cylindrical object ($\mu = 0.7$).

wedge–effect is blocked under a significant surface friction. Therefore, we need an alternative strategy for enveloping the object under a significant friction.

When the robot recognizes any failure, it switches grasping strategy from sliding to rolling based strategies after putting down the object on the table. Fig.2.17 shows an example of *rolling based grasp*.

Task 1 (Detaching motion)	**: Rolling motion**
Task 2 (Lifting motion)	**: Rolling motion**
Task 3 (Grasping motion)	**: Constant torque command**

○ **Group–C_1 : Regrasping based grasp**

$$(d_{robot} < (\pi D_{tip})/L_r \ \cap \ \textit{Contact friction is small}\ )$$

For an object whose diameter is small enough to ensure that any fingertip can not

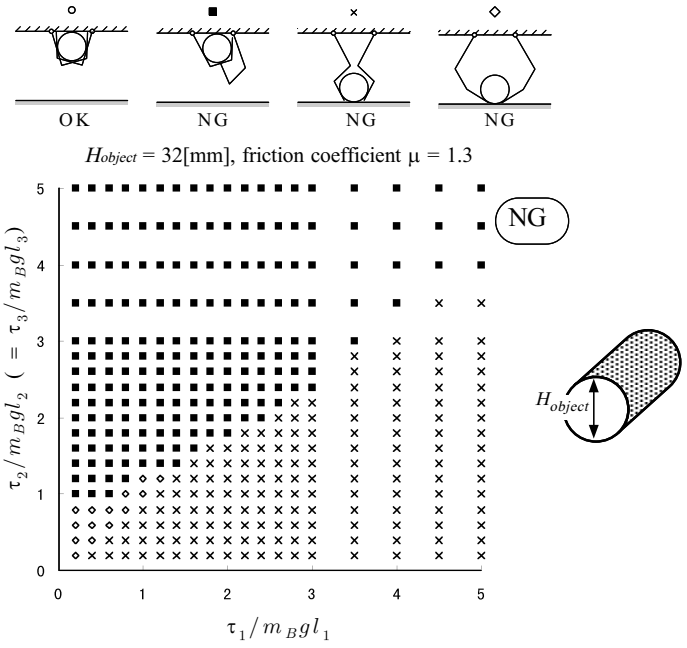

Fig. 2.16: Success map for a cylindrical object ($\mu = 1.3$).

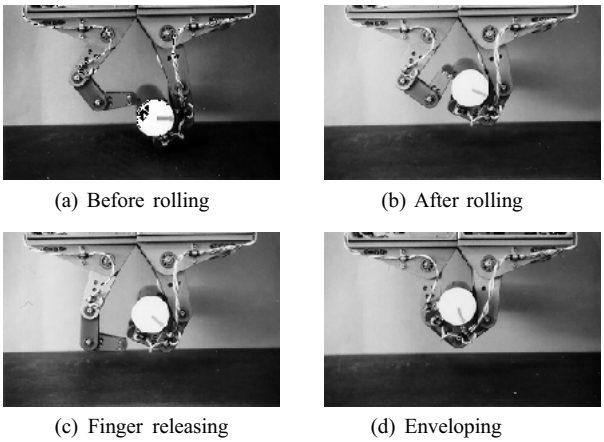

Fig. 2.17: Rolling based grasp.

be inserted into the bottom part of object, it becomes difficult to utilize the *wedge–effect*. In such a case, *regrasping based grasp* may be an appropriate strategy for finally enveloping the object. *Regrasping based grasp* can be decomposed of two basic motions where one is the motion for picking up the object by using two fingers as shown in Fig.2.18(a), and the other one is the regrasping motion as shown in Fig.2.18(b) through

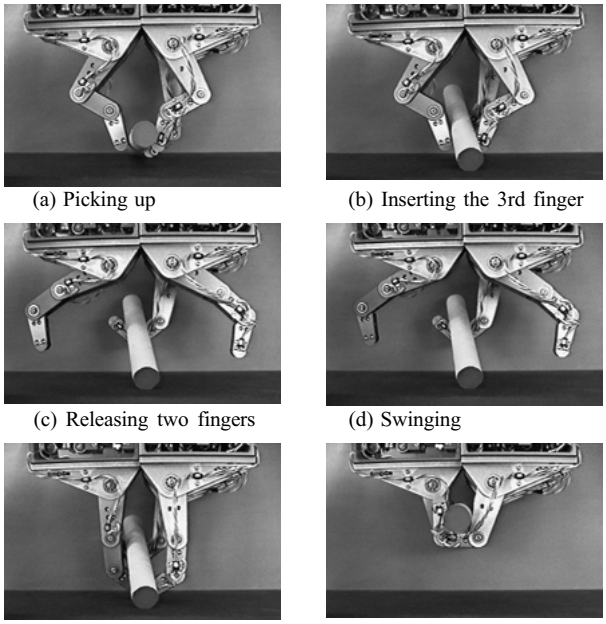

(a) Picking up (b) Inserting the 3rd finger

(c) Releasing two fingers (d) Swinging

(e) Regrasping (f) Enveloping

Fig. 2.18: Regrasping based grasp.

(e). The first motion plays an important role in allowing no interference from the table. In the following motion, the remaining finger hooks the object so that we can make a small gap between the object and the table as shown in Fig.2.18(b), even though two fingers picking up the object are released from the object. After these finger motions, the object is supported by one finger and the table as shown in Fig.2.18(c). We note that under such object's posture we can find an enough space between the object and the table for inserting the released fingers. In the next step, the left finger is swung a bit as shown in Fig.2.18(d) so that both the right and the left fingers may not interfere with each other during the finger closing motion. After every finger is inserted into the bottom of object as shown in Fig.2.18(e), constant torque control is applied for achieving an enveloping grasp as shown in Fig.2.18(f). While human regrasps the object in the air, the robot hand uses the surface of table effectively in order to prevent the object from falling down.

Task 1 (Detaching motion)	**: Alternative finger inserting motion**
Task 2 (Lifting motion)	**: Constant torque command**
Task 3 (Grasping motion)	**: Constant torque command**

◯ **Group–C_2 : Regrasping based grasp with Rolling motion**

$(d_{robot} < (\pi D_{tip})/L_r \ \cap$ *Contact friction is large*)

For an object satisfying this condition, the regrasping motion just same as the motion for Group–C_1 (*Regrasping based grasp*) can be applied for detaching the object from the table and inserting the finger into the bottom of object. However, the object can not slide over the finger link surface under a large contact friction. Thus, after detaching the object from the table, a rolling motion utilized in Group–B_2 (*Rolling based grasp*) is applied for carrying the object to the palm.

Task 1 (Detaching motion)	**: Alternative finger inserting motion**
Task 2 (Lifting motion)	**: Rolling motion**
Task 3 (Grasping motion)	**: Constant torque command**

2.3.5 With Initial Adjustment Motion : Group–D_2

For an object whose cross–section shape is circle as shown in Fig.2.19(a), an upward force can be produced by pushing the bottom of the object towards the horizontal direction. For an object whose cross–section shape is triangle or rectangle as shown in Fig.2.19(b), the fingertip forces may produce a downward force or balance each other within the object. Under such a situation, the lifting force is not produced even though the contact force is increased. From grasp experiments by human, the rotating motion is obviously a key for detaching an object from the table if it has rectangular or triangular cross–section. For either object, a robot hand also conveniently utilizes the

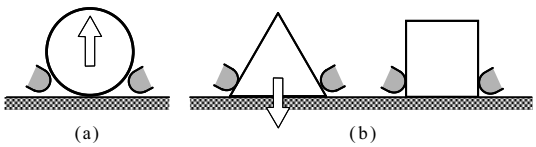

Fig. 2.19: Examples of objects where the upward force is expected (a) and is not expected (b) by a simple pushing motion.

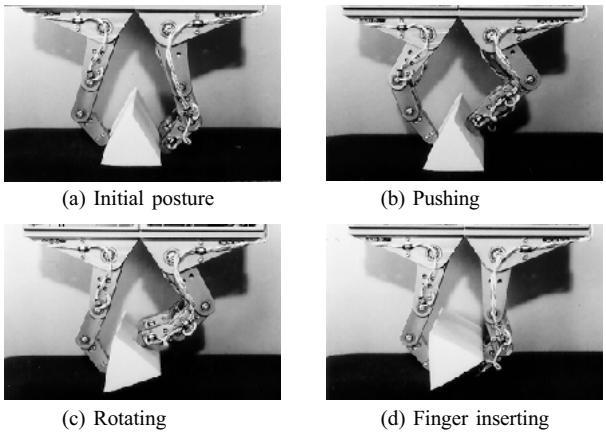

Fig. 2.20: Initial adjustment motion (Rotating motion).

rotating motion for producing a space for inserting fingers between the object and the table. For this *initial adjustment motion* we can also apply the toppling manipulation where the rotating motion is guaranteed by just one finger[36]. Fig.2.20 shows an example of the *initial adjustment motion*. Once a sufficient gap is produced as shown in Fig.2.20(c), one finger is removed away from the object's surface and inserted into the gap as shown in Fig.2.20(d). After the fingertip is inserted into the gap between the object and the table, we apply the same grasping mode as those taken for cylindrical objects.

2.3.6 The Switching Algorithm for Grasping Strategy

We now discuss how to choose an appropriate one from various strategies prepared according to the size, cross–section shape, and contact friction of objects, and how to

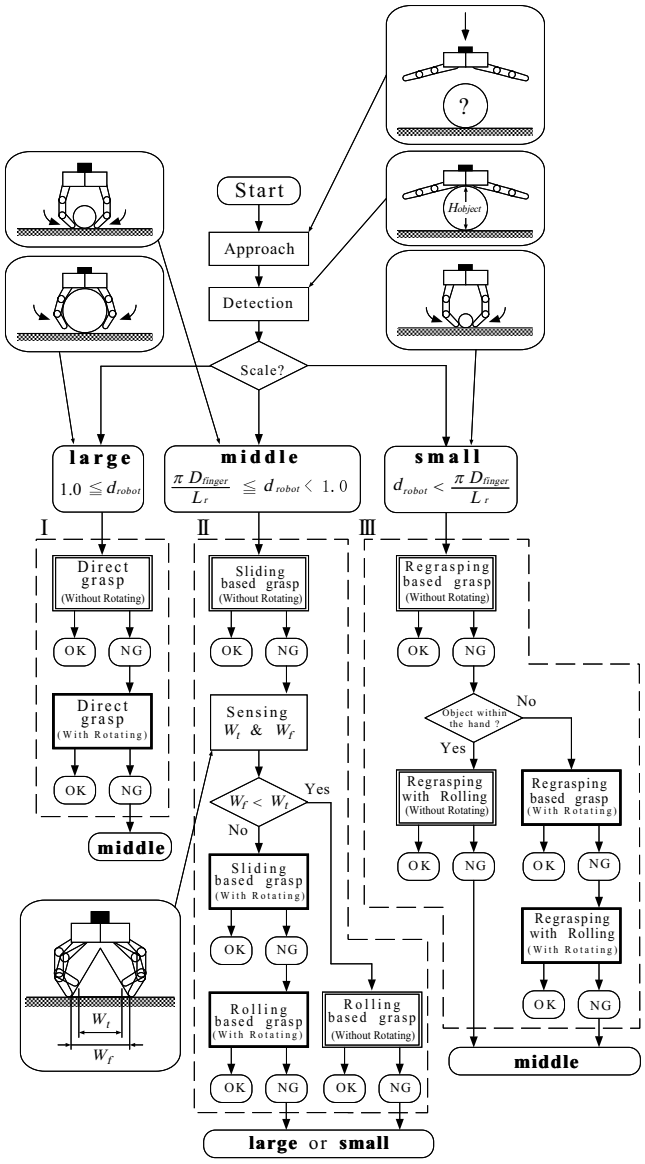

Fig. 2.21: The strategy flow–diagram.

switch from one to another when a robot hand fails in grasping an object. First of all, a robot hand needs to know the size of object, so that it can choose a strategy appropriate for the scale. An appropriate candidate is to utilize a tactile sensor installed in the palm. Suppose that each finger is fully opened initially and we make the hand come down until either the palm sensor or the finger link makes contact with an object. By

this contact, the robot can detect the height of object H_{object} and d_{robot} computed by $\pi H_{object}/L_r$. While πH_{object} does not provide the circumference of object in general, it denotes the exact one for a cylindrical object. Anyway, the robot can roughly estimate the size of object by $\pi H_{object}/L_r$. Even for two objects having the same d_{robot}, there are some cases where two different strategies exist. In such a case, we take the idea of *Easier–Strategy–Comes–First* which starts from the easier strategy and switches into the other one when an easy one fails. Fig.2.21 shows the *strategy flow–diagram*, where relatively complicated strategies are placed in lower parts and strategies surrounded by a bold line entail the *initial adjustment motion*.

The strategy block–I consists of *direct grasp*. It is difficult that the robot hand lifts up a triangular or a rectangular object from the table by the *direct grasp without rotating motion*, except for the case that the contact friction is large. In such a case, the robot hand applies the *direct grasp with rotating motion*. When the robot hand fails in grasping the object, it estimates that the object is small for achieving the *direct grasp*, then it switches the block–I to the block–II.

The strategy block–II consists of *sliding* and *rolling based grasps*. At first, the robot hand tries the *sliding based grasp* since it is simpler than the *rolling based grasp*. When the contact friction is large, the robot hand can not utilize the *sliding based grasp*. When the cross–section shape of object has triangle or rectangle, the robot hand needs the *initial adjustment motion* before further steps. Based on the *success condition of enveloping grasp*, the robot hand recognizes the failure. In either case that the object has triangular or rectangular cross–section, the *initial adjustment motion* is necessary before starting Task 1 through 3. Therefore, the robot hand needs the information concerning the cross–section shape of the object when it recognizes the failure. While

the robot needs the bottom shape of object, it is not necessary for the robot to know the full cross–section shape for choosing an appropriate strategy. The bottom shape of object can be estimated by measuring width W_f and W_t, where W_f and W_t are the width at the bottom and the width at a bit higher position as shown in Fig.2.21, respectively. If $W_f < W_t$, cross–section shapes are, for example, pentagon, hexagon, circle, and so on. When the robot fails in grasping under $W_f < W_t$, it judges a large contact friction of object. Based on this estimation, the robot hand chooses the *rolling based grasp*. On the other hand, if $W_f \geq W_t$, the cross–section shape should be triangle or rectangle. In case of $W_f \geq W_t$, the robot hand chooses the *sliding based grasp with rotating motion*. If both approaches in block–II do not work successfully, the robot hand switches the strategy block to either block–I or block–III.

The strategy block–III consists of *regrasping based grasp*. First, the robot hand tries the *regrasping based grasp*. When the robot hand fails in grasping, it checks the status where the object is. When the object is in the robot hand, it switches the strategy to the *regrasping based grasp with rolling motion* according to the reasoning that the contact friction is too large for lifting up the object by utilizing constant torque control. On the other hand, when the object is not detached from the table, the robot hand switches the strategy to the *regrasping based grasp with rotating motion* according to the reasoning that the object is triangular or rectangular column. When all strategies in block–III do not work appropriately, the robot hand switches the strategy block to the block–II.

While the switching in the *strategy flow–diagram* given in Fig.2.21 is based on tactile information, each block becomes much simpler under a vision sensor.

2.3.7 Toward General Column Objects

For a general column objects, the most important point is to confirm whether the robot hand can detach the object from the table or not (Task 1).

Let β_1 and β_2 be angles between an edge of the object and the table as shown in Fig.2.22. We classify general column objects into three groups where both β_1 and β_2 are greater than $\pi/2[rad]$ in (a), either β_1 or β_2 is greater than $\pi/2[rad]$ in (b), and both β_1 and β_2 are less than $\pi/2[rad]$ in (c), respectively. For an object shown in (a), we can apply the same grasping strategy as those used for a cylindrical object. The objects classified into Fig.2.22(b) are not included in the *strategy flow–diagram*. Now, suppose that two fingers push the bottom part of object as shown in Fig.2.23(a). While the right finger does not contribute to lifting up the object, the left finger produces the *wedge–effect* and rotates the object around one edge of the object as shown in Fig.2.23(b). If the surface friction is small enough, the hand will lift up the object by sliding motion and finally complete the enveloping grasp. Thus, the object shown in Fig.2.22(b) can be included in the same group which can be achieved by the *sliding based grasp* if the contact friction is small. Now, let us consider an object classified into the group in Fig.2.22(c). Such an object needs the *initial adjustment motion* requested for either a triangular or a rectangular objects. For achieving the *initial adjustment motion*, the robot has to detect $\boldsymbol{p}_{top}$ where the rotating moment is produced as far as the contact friction is not zero. Since $\boldsymbol{p}_{top}$ does not always exist for general column objects, the robot often meets an object where $\boldsymbol{p}_{top}$ is not found. In such a case, the robot anyway pushes at $\boldsymbol{p}'_{top}$ where $\boldsymbol{p}'_{top}$ denotes the top of object as shown in Fig.2.23(c). When the robot can not rotate the object, it gives up grasping the object.

As far as the surface friction is large enough, the robot hand can not grasp the object

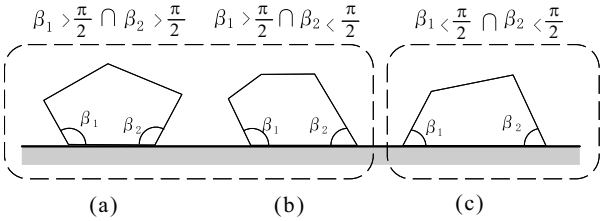

Fig. 2.22: Grouping of column objects whose cross–section shapes are convex.

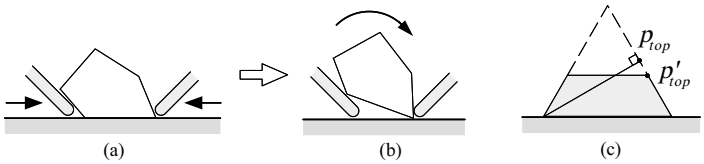

Fig. 2.23: The wedge–effect at one edge of the object.

whose shape is extremely flat, and both β_1 and β_2 are smaller than $\pi/2[rad]$, while it can grasp an object if $\pi/2 < \beta_1$ and $\pi/2 < \beta_2$. In other words, if the robot hand can not find any contact points which can produce upward force, it can not grasp the object firmly in the air.

2.3.8 Summary

We proposed five basic grasping strategies (*direct grasp, sliding based grasp, rolling based grasp, regrasping based grasp, initial adjustment motion*) which are easily applicable for general multi–fingered robot hands. We discussed the *guide–line–map* for choosing an appropriate strategy among these strategies according to the size, cross–section shape, and contact friction of object. We also showed the *strategy flow–diagram* to explain how to switch grasping strategy from one to another when the robot hand fails in grasping the object. We also relaxed the assumptions, so that we can pursue the generality of the grasping strategy.

2.4 Discussion

For cylindrical objects with $d_{robot} \leq (\pi D_{tip})/L_r$, we can prepare similar grasp strategies that human are taking. However, for a small cylindrical object, it is extremely difficult for a robot hand to achieve the target grasp by applying a series of grasp motions that human do. Especially, it is hard for a robot to realize the transition phase from the fingertip grasp to the enveloping grasp in the air. To cope with this, we apply an alternative strategy, *regrasping based grasp*, where the robot utilizes the table as much as possible. This strategy releases us from worrying about dropping the object. However, the proposed approach is still too complicated to keep a high success rate. Keeping this point in mind, we pursue a further simple grasping strategy in chapter 3 through human observation.

Chapter 3

Discovery of Detaching Assist Motion (DAM)

3.1 Introduction

In this chapter, we focus on cylindrical objects whose diameter is relatively small as shown in Fig.3.1. From the viewpoint that how human captures such a small object within the hand, let us once again observe human behavior for grasping a small cylindrical object, so that we can obtain a clue for simplifying the grasp strategy for a robot hand.

3.2 Human Observation

In addition to the grasping pattern as shown in Fig.3.1(a) we newly found an interesting one as shown in Fig.3.1(b), where human first approaches the object until fingertips make contact with the object, and then the finger posture is changed from upright to curved ones gradually. We call a series of motions *Detaching Assist Motion (DAM)*. From the viewpoint of robot application, the most attractive feature of *DAM* is its extremely simple finger motion, while the grasp pattern in Fig.3.1(a) is so complicated

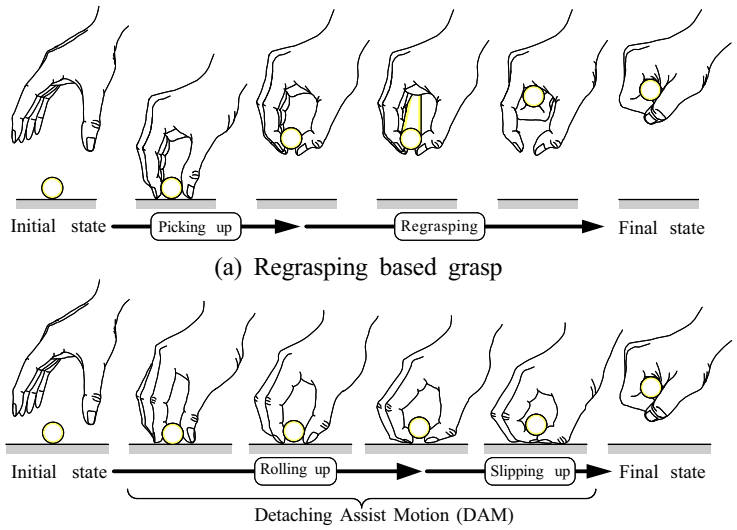

(a) Regrasping based grasp

(b) Detaching Assist Motion

Fig. 3.1: Two grasp patterns for enveloping a cylindrical object placed on a table

that the robot hand may often fail especially in changing the phase from the fingertip to the enveloping grasp. The second advantage is that the *DAM* is achieved on the table in most phases and, therefore, it is not necessary to worry about dropping the object.

Why does the *DAM* work effectively for detaching the object from the table? What kind of principle exists behind it? In this chapter, to clarify the basic working mechanism of *DAM*, we examine both finger posture and object position while human purposely applies the *DAM* as shown in Fig.3.1(b). The seven markers are attached at the side of object and each joint of index finger and thumb as shown in Fig.3.2(a). We measure the coordinates of markers from the video image sequences recorded by video camera system, where the sampling time is $1/30[sec]$. The angular displacement of each joint and the center of gravity of object can be obtained from the image sequences.

Figs.3.2(b) through (f) show experimental results for a cylindrical object with the diameter of $8[mm]$, while human utilizes the *DAM* from the initial posture to the final

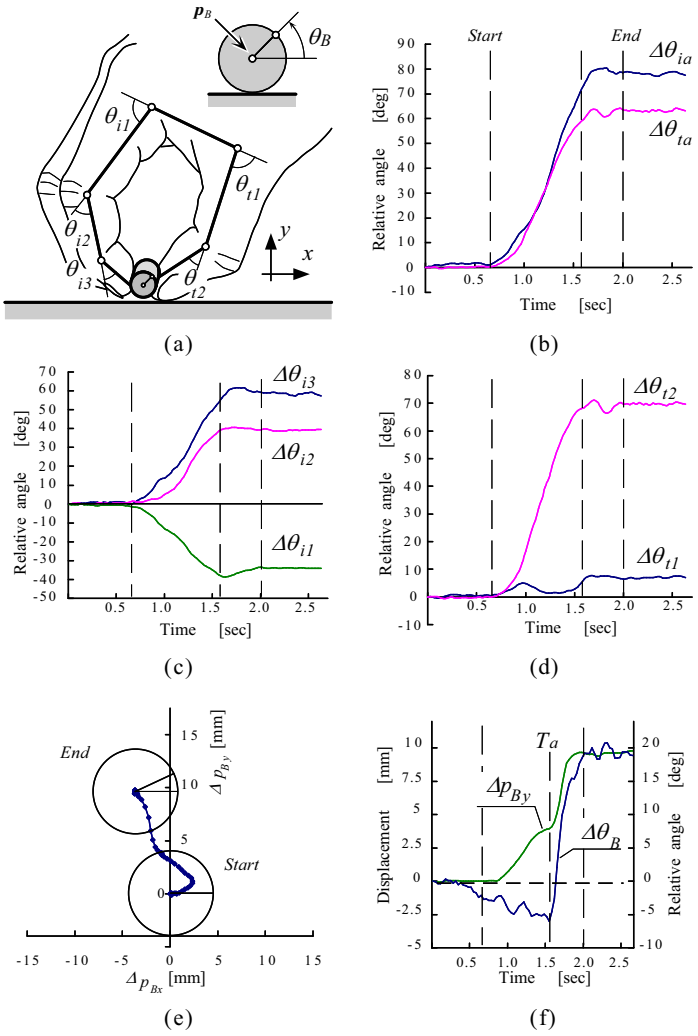

Fig. 3.2: Visual observation during DAM

posture, where Figs.3.2(b),(c),(d),(e) and (f) show the changes of $\Delta\theta_{ia}$ and $\Delta\theta_{ta}$, the changes of $\Delta\theta_{i1}$, $\Delta\theta_{i2}$ and $\Delta\theta_{i3}$, the changes of $\Delta\theta_{t1}$ and $\Delta\theta_{t2}$, the trajectory of $\boldsymbol{p}_B$ and the change of Δp_{By} and $\Delta\theta_B$, respectively. From Fig.3.2(b), it can be seen that both fingertips rotate uniformly with respect to time and finally keep constant in posture. An interesting behavior appears for the object motion when $t = 1.57[sec](= T_a)$. At the moment of T_a, the object suddenly starts to move up with rotating motion as shown in Fig.3.2(f), while it slowly moves before T_a.

3.3 The Basic Working Mechanism of DAM

Let us discuss what is really happening during the *DAM* by using the fingertip model as shown in Fig.3.3. We assume that the object is small enough to ensure that a simple pushing motion in the horizontal direction can not lift up the object as shown in Fig.3.3(a). Now, for simplifying the discussion, let us simplify the fingertip model as shown in Fig.3.3(b). Before T_a, we can observe from video image that the object and the fingertip keep the rolling contact. If we can assume that each fingertip does not slip on the surface of object, both fingertips will rotate from the initial to the final postures according to the geometrical restriction between finger and object as shown in Fig.3.3(b) and (c). We call this phase *Rolling–up phase*. As the object is lifted up, the normal direction of friction cone gradually changes upwards while the contact point moves towards the bottom of object. Finally, the moment the contact force is away from the friction cone, the object slips on the surface of fingertips, and the *wedge–effect* occurs as shown in Fig.3.3(d). Once the contact force is away from the boundary, the *wedge–effect* can be continuously expected. We can also observe from video image that the fingertips of index finger and thumb slip simultaneously the moment of T_a. This is basic mechanism why the object suddenly moves upwards after T_a. We call the final phase *Wedge–effect phase*. These are the outline of the basic working mechanism of *DAM*. The phase from *Rolling–up* to *Wedge–effect* is automatically switched depending upon the finger rotating motion.

3.4 Summary

We newly found the *DAM* through the observation of human grasping motion. We analyzed the finger posture during the *DAM* and explained the basic working mechanism

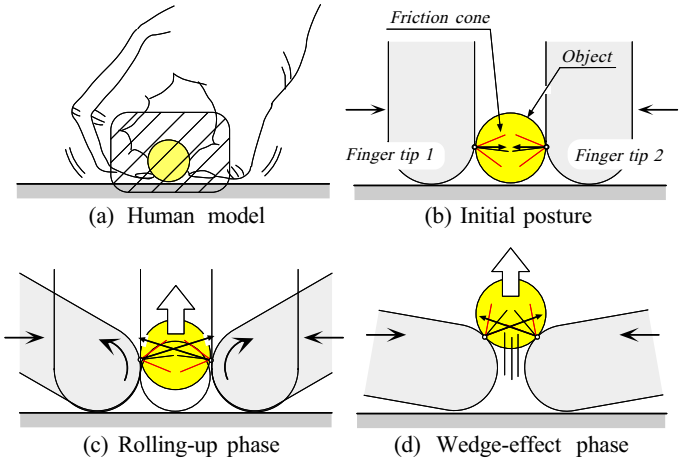

Fig. 3.3: The basic working mechanism of DAM

of *DAM*. Since the *DAM* can be achieved by an extremely simple finger motion and manipulate the object in most phases on the table, we believe that it can be easily applied to multi–fingered robot hands.

Chapter 4

Implementation of DAM into Robot Hand

4.1 Introduction of SPCM

Our goal in this chapter is to analyze the *DAM*, especially to explore under what condition a robot hand can lift up an object from a table. During the *DAM*, either sliding or rolling motion may happen at the contact point. We do not care what kinds of motion occur but are interesting only to know whether the object is lifted up or not. While several strategies for robot hands which are equivalent to the *DAM* by human can be considered, we utilize compliant motion of link system having one compliant joint (s_i-th) and one position–controlled joint (p_i-th) as shown in Fig.4.1(a). Now, suppose that we impart an arbitrary angular displacement $\Delta\theta_{pi}$ at the position–controlled joint p_i for such a link system contacting with an environment. Under the condition, the link system will automatically change its posture while keeping contact between the environment and the link system, if $\Delta\theta_{pi}$ is given appropriately. This series of motions is termed as *Self–Posture Changing Motion (SPCM)*[15], [38]. *SPCM* has been conveniently utilized for detecting an approximate contact point between a

link system and an unknown object under the assumption that the object does not move during sensing motion. For example, let us consider two different link postures during *SPCM*. Between two link postures, we can always find an intersection, which provides us with an approximate contact point. This approach allows us to detect an approximate contact point without implementing any tactile sensor, which is a great advantage. In this work, however, we allow the object to move according to the contact force imparted by the link as shown in Fig.4.1(b).

[Definition of *SPCM*]

For a link system with m_i joints, suppose that the s_i-*th* joint of i-*th* finger is compliant and $h_i(> s_i)$-*th* link makes contact with an object, and the angular displacement,

$$|\Delta\theta_{pi}| \neq 0 \tag{4.1}$$

is imparted at the position–controlled joint p_i $(h_i \geq p_i > s_i)$. If the vector $\boldsymbol{p}_{Ci} \in R^{3\times 1}$ satisfying the following equations is always found during a change of link posture, we call there exists *Self–Posture Changeability (SPC)*.

$$S_B({}^B\boldsymbol{p}_{CBi}) = 0, \quad S_{Fi}({}^{Fi}\boldsymbol{p}_{CFi}) = 0 \tag{4.2}$$

$$\boldsymbol{p}_B + \boldsymbol{R}_B{}^B\boldsymbol{p}_{CBi} = \boldsymbol{p}_{Fi} + \boldsymbol{R}_{Fi}{}^{Fi}\boldsymbol{p}_{CFi} = \boldsymbol{p}_{Ci} \tag{4.3}$$

$$\boldsymbol{n}_{CBi} = -\boldsymbol{n}_{CFi} \tag{4.4}$$

The series of motions that bring about a *SPC* is defined as a *Self–Posture Changing Motion (SPCM)* and we express it as $SPCM\{k_{\theta i}, \Delta\theta_{pi}\}$, where $k_{\theta i}$ is the joint stiffness of the s_i-*th* joint of i-*th* finger.

In *SPCM*, the h_i-*th* link always keeps contact with the object during the change of link posture. From the basic behavior, we can see that it is almost equivalent to the *DAM* by human. The *SPCM* has an advantage where it can achieve with, at least, one

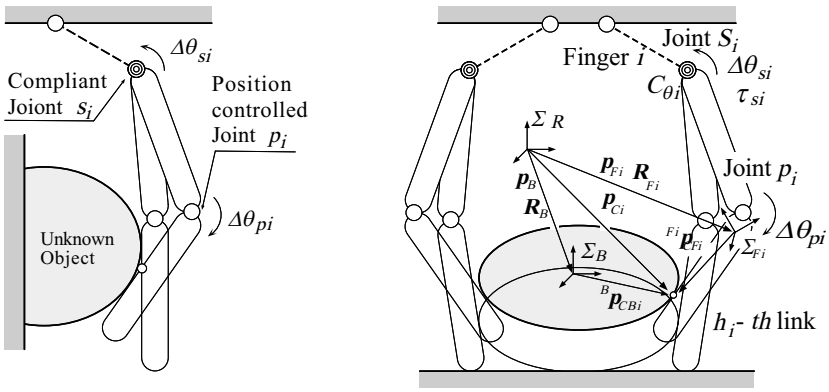

(a) Object is fixed (b) Object's motion is allowed

Fig. 4.1: Self-Posture Changing Motion

compliant joint and one position–controlled joint at each finger without complicated motion planning.

4.2 Conditions for Lifting up an Object

4.2.1 Problem Formulation

Now, we discuss a condition for lifting up an object by utilizing the *SPCM*. Suppose that the robot hand utilizes $SPCM\{\boldsymbol{K}_\theta, \Delta\boldsymbol{\theta}_p\}$ for the object whose mass is m_B, where we use $\boldsymbol{K}_\theta = diag[k_{\theta 1}, \ldots, k_{\theta n}] \in R^{n\times n}$ and $\Delta\boldsymbol{\theta}_p = [\Delta\theta_{p1}, \ldots, \Delta\theta_{pn}]^t \in R^{n\times 1}$ for multiple fingers instead of $k_{\theta i}$ and $\Delta\theta_{pi}$. Let $\boldsymbol{f}_c = [\boldsymbol{f}_{c1}^t, \ldots, \boldsymbol{f}_{cn}^t]^t \in R^{3n\times 1}$ and $\boldsymbol{W}_{ext} \in R^{6\times 1}$ be the contact force vector at each contact point and the load wrench, respectively. The equation of the force and the moment balancing on the object can be expressed as

$$\boldsymbol{W}_{ext} = -\boldsymbol{G}^t \boldsymbol{f}_c, \tag{4.5}$$

where $\boldsymbol{G}^t \in R^{6\times 3n}$ is the grasp matrix and given by

$$\boldsymbol{G}^t = \begin{bmatrix} \boldsymbol{I}_3 & \cdots & \boldsymbol{I}_3 \\ (\boldsymbol{R}_B{}^B\boldsymbol{P}_{CB1}\times) & \cdots & (\boldsymbol{R}_B{}^B\boldsymbol{P}_{CBn}\times) \end{bmatrix}.$$

Suppose that the load wrench is $\boldsymbol{W}_{ext} = [0, 0, -(m_B g + f_{ez}), 0, 0, 0]^t$, where g and f_{ez} are the acceleration of gravity and the virtual force in the gravitational direction at the center of gravity of object, respectively. Any component of $\boldsymbol{f}_c$ can not exist outside of the friction cone at each contact point. If all components of $\boldsymbol{f}_c$ exist inside of the friction cone with $f_{ez} = 0$, the object does not move since the resultant force acting on the object balances within the object. If the resultant force does not balance without pushing down by an additional force $f_{ez} > 0$, the object is necessarily lifted up from the table when such a virtual external force f_{ez} is removed. Based on this consideration, we can summarize the problem as follows.

[Problem formulation]

Search $SPCM\{\boldsymbol{K}_\theta, \Delta\boldsymbol{\theta}_p\}$ where the contact force $\boldsymbol{f}_c$ balances with $\boldsymbol{W}_{ext}$ by utilizing a virtual external force $f_{ez} \geq 0$.

4.2.2 A Sufficient Condition

All compliant joints rotate $\Delta\boldsymbol{\theta}_s$ according to the angular displacement $\Delta\boldsymbol{\theta}_p$ under the assumption that the object does not move for an $SPCM\{\boldsymbol{K}_\theta, \Delta\boldsymbol{\theta}_p\}$. Under the $SPCM\{\boldsymbol{K}_\theta, \Delta\boldsymbol{\theta}_p\}$, $\boldsymbol{\tau}_s = -\boldsymbol{K}_\theta \Delta\boldsymbol{\theta}_s (= \boldsymbol{\tau}_{bias})$, where $\boldsymbol{\tau}_s = \mathbf{o}$ is assumed in the initial state. The relationship between τ_{si} and $\boldsymbol{f}_{ci}$ is given by $\tau_{si} = \boldsymbol{J}_i^t \boldsymbol{f}_{ci}$ where $\boldsymbol{J}_i^t \in R^{1\times 3}$ denotes the Jacobian matrix mapping from $\boldsymbol{f}_{ci}$ to τ_{si}. The contact force $\boldsymbol{f}_{ci}$ can be solved

$$\boldsymbol{f}_{ci} = (\boldsymbol{J}_i^t)^{\#} \tau_{si} + [\boldsymbol{I}_3 - (\boldsymbol{J}_i^t)^{\#} \boldsymbol{J}_i^t] \boldsymbol{w}_i \tag{4.6}$$

where $\boldsymbol{w}_i \in R^{3\times 1}$, $\boldsymbol{I}_3 \in R^{3\times 3}$ and $\#$ are an arbitrary vector, the identical matrix and the seudo–inverse matrix, respectively. τ_{si} is automatically determined when both $\boldsymbol{K}_\theta$ and $\Delta\boldsymbol{\theta}_p$ are given. The first term in eq.(4.6) denotes the force component perpendicular to both the unit axis vector of compliant joint and the vector indicating from the compliant joint to the contact point. The second term in eq.(4.6) is perpendicular to $(\boldsymbol{J}_i^t)^{\#} \tau_{si}$ and can take an arbitrary value within the friction cone.

Now, we consider the frictional constraint. In order to change from nonlinear to liner constraint, a friction cone is often modeled by the L–faced polyhedral convex cone[39][40] whose span vectors are expressed by $\boldsymbol{v}_i^1, ..., \boldsymbol{v}_i^L$ as shown in Fig.4.2, respectively. The contact force for the *i-th* finger is given by

$$\boldsymbol{f}_{ci} = \boldsymbol{V}_i \boldsymbol{\lambda}_i \tag{4.7}$$

where $\boldsymbol{\lambda}_i = [\lambda_i^1, ..., \lambda_i^L]^t \in R^{L\times 1}$ and $\boldsymbol{V}_i = [\boldsymbol{v}_i^1, ..., \boldsymbol{v}_i^L] \in R^{3\times L}$. Therefore, the torque of compliant joint is expressed by

$$\tau_{si} = \boldsymbol{J}_i^t \boldsymbol{V}_i \boldsymbol{\lambda}_i \tag{4.8}$$

For n fingers, we obtain

$$\boldsymbol{\tau}_s = \boldsymbol{J}^t \boldsymbol{V} \boldsymbol{\lambda} \tag{4.9}$$

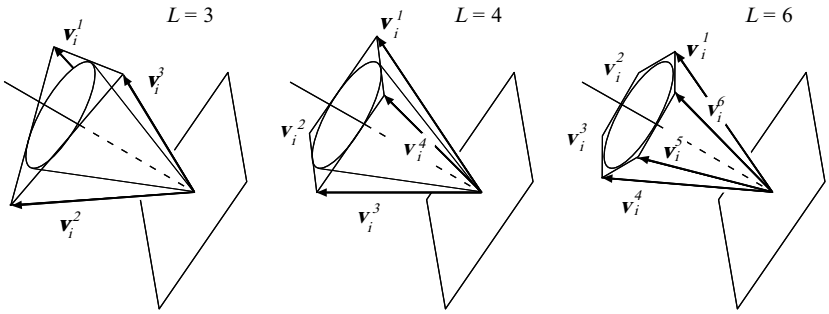

Fig. 4.2: Approximation of the friction cone to L-faced polyhedral convex cone.

By solving eq.(4.9) with respect to $\boldsymbol{\lambda} = [\boldsymbol{\lambda}_1^t, ..., \boldsymbol{\lambda}_n^t]^t \in R^{Ln\times 1}$,

$$\boldsymbol{\lambda} = \boldsymbol{H}^{\#}\boldsymbol{\tau}_s + (\boldsymbol{I}_{Ln} - \boldsymbol{H}^{\#}\boldsymbol{H})\boldsymbol{u} \tag{4.10}$$

where

$$\boldsymbol{H} = \begin{bmatrix} \boldsymbol{J}_1^t\boldsymbol{V}_1 & & \mathbf{o} \\ & \ddots & \\ \mathbf{o} & & \boldsymbol{J}_n^t\boldsymbol{V}_n \end{bmatrix} \in R^{n\times Ln},$$

$\boldsymbol{u} \in R^{Ln\times 1}$ denotes an arbitrary vector. Eq.(4.10) can be rewritten as follows,

$$\boldsymbol{\lambda} = \boldsymbol{H}^{\#}\boldsymbol{\tau}_s + \boldsymbol{N}\boldsymbol{\Phi} \tag{4.11}$$

where $\boldsymbol{\Phi} \in R^{(L-1)n\times 1}$ is an arbitrary vector and $\boldsymbol{N} \in R^{Ln\times(L-1)n}$ is the full rank matrix satisfying $\boldsymbol{H}\boldsymbol{N} = \mathbf{o}$. As a result, the total force of the center of gravity of object $\boldsymbol{f}_o \in R^{3\times 1}$ is expressed by

$$\boldsymbol{f}_o = \boldsymbol{E}\boldsymbol{V}\{\boldsymbol{H}^{\#}\boldsymbol{\tau}_s + \boldsymbol{N}\boldsymbol{\Phi}\} \tag{4.12}$$

where $\boldsymbol{E} = [\boldsymbol{I}_3, ..., \boldsymbol{I}_3] \in R^{3\times 3n}$. We focus on the contact force coinciding with a span vector, when discussing the boundary of total force set[41]. We introduce the following two constraints.

$$\boldsymbol{S}\boldsymbol{\lambda} \geq \mathbf{o} \tag{4.13}$$

$$\boldsymbol{S}^*\boldsymbol{\lambda} = \mathbf{o}, \tag{4.14}$$

where $\boldsymbol{S} = diag[\boldsymbol{e}_{1k}^t, ..., \boldsymbol{e}_{nk}^t] \in R^{n \times nL}$, $\boldsymbol{S}^* = diag[\boldsymbol{\Gamma}_1, ..., \boldsymbol{\Gamma}_n] \in R^{n(L-1) \times nL}$, $\boldsymbol{\Gamma}_i = [\boldsymbol{e}_i^1, ..., \boldsymbol{e}_i^{(k-1)}, \boldsymbol{e}_i^{(k+1)}, ..., \boldsymbol{e}_i^L]^t \in R^{(L-1) \times L}$. Ineq.(4.13) is for keeping each contact force in the pushing direction for the object, and eq.(4.14) is for making each contact force adhere to one ridge. These constraints mean that each contact force adhere to one of span vectors. Since $\boldsymbol{S}^*$ and $\boldsymbol{N}$ are full rank, $\boldsymbol{S}^*\boldsymbol{N}$ becomes a nonsingular matrix. From eqs.(4.11) and (4.14)

$$\boldsymbol{\Phi} = -\boldsymbol{D}^{-1}\boldsymbol{S}^*\boldsymbol{H}^{\#}\boldsymbol{\tau}_s, \tag{4.15}$$

where $\boldsymbol{D} = \boldsymbol{S}^*\boldsymbol{N}$.

Substituting $\boldsymbol{\Phi}$ into eq.(4.12) yields

$$\boldsymbol{f}_o = \boldsymbol{E}\boldsymbol{V}(\boldsymbol{I} - \boldsymbol{N}\boldsymbol{D}^{-1}\boldsymbol{S}^*)\boldsymbol{H}^{\#}\boldsymbol{\tau}_s. \tag{4.16}$$

A sufficient condition for lifting up the object is to find $\boldsymbol{\tau}_s$ satisfying the following inequality for all possible combinations of contact forces.

$$0 < \boldsymbol{c}_z^t \boldsymbol{f}_o - m_B g, \tag{4.17}$$

where $\boldsymbol{c}_z = [0, 0, 1]^t$ is the unit vector indicating the direction of z-axis in Σ_R.

Also these formulations can be applied for other link mechanisms such as legged robots[57].

4.2.3 Contact Stiffness Model Based Approach

The relationship between $\boldsymbol{f}_c$ and $\boldsymbol{\tau}_s$ is expressed as follows,

$$\boldsymbol{\tau}_s = \boldsymbol{J}^t \boldsymbol{f}_c, \tag{4.18}$$

where $\boldsymbol{J}^t \in R^{n\times 3n}$ denotes the Jacobian matrix mapping from $\boldsymbol{f}_c$ to $\boldsymbol{\tau}_s$. Therefore, the relationship among $\boldsymbol{f}_c$, $\boldsymbol{W}_{ext}$ and $\boldsymbol{\tau}_s$ can be expressed as eq.(4.19).

$$\begin{bmatrix} \boldsymbol{W}_{ext} \\ \boldsymbol{\tau}_s \end{bmatrix} = \begin{bmatrix} -\boldsymbol{G}^t \\ \boldsymbol{J}^t \end{bmatrix} \boldsymbol{f}_c \tag{4.19}$$

Bicchi[42], [43], Zhang, Gao and Gruver[44], Omata and Nagata[21] pointed out that eq.(4.19) contains the indeterminate contact force which neither affects $\boldsymbol{\tau}_s$ nor appears in $\boldsymbol{W}_{ext}$. While Omata and Nagata have analyzed the indeterminate grasp force by considering that sliding directions are constrained in power grasps, the algorithm for finding the range requires a complicated procedure. To cope with this problem, we put an assumption:

(A4-1) There is an extremely small compliance at each contact point between each finger and the object.

This assumption releases us from such an indeterminate contact force, since the contact force $\boldsymbol{f}_c$ is uniquely determined under the contact stiffness $\boldsymbol{K}_P = diag[\boldsymbol{K}_{P1}, \ldots, \boldsymbol{K}_{Pn}] \in R^{3n\times 3n}$ at the contact point as shown in Fig.4.3, where

$$\boldsymbol{K}_{Pi} = \begin{bmatrix} k_{ixx} & k_{ixy} & k_{ixz} \\ k_{iyx} & k_{iyy} & k_{iyz} \\ k_{izx} & k_{izy} & k_{izz} \end{bmatrix} \in R^{3\times 3}. \tag{4.20}$$

This approach is often taken in conventional works[42]–[46].

We assume the displacement $\delta\boldsymbol{x} \in R^{6\times 1}$ and $\delta\boldsymbol{\theta}_s \in R^{n\times 1}$ under an external wrench $\boldsymbol{w}_{ext}$, where $\delta\boldsymbol{x}$ and $\delta\boldsymbol{\theta}_s$ denote the vector expressing the displacement and the rotation of object and the angular displacement of compliant joints. Now, the relationship among displacement vectors $\delta\boldsymbol{P}$, $\delta\boldsymbol{x}$, and $\delta\boldsymbol{\theta}_s$ is given by

$$\delta\boldsymbol{P} = \boldsymbol{G}\delta\boldsymbol{x} - \boldsymbol{J}\delta\boldsymbol{\theta}_s, \tag{4.21}$$

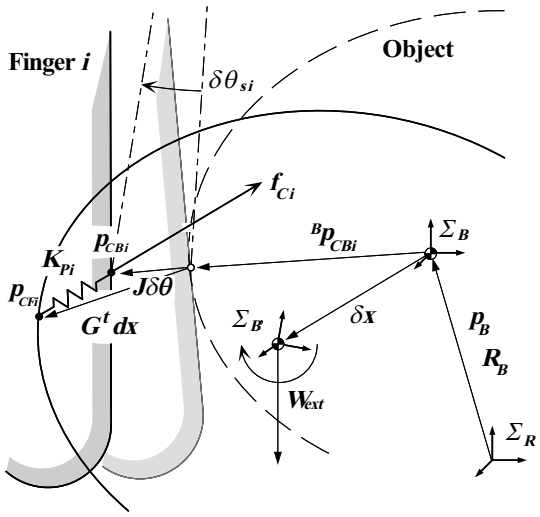

Fig. 4.3: Contact stiffness model

where $\delta \boldsymbol{P} = [\delta \boldsymbol{P}_1^t, \ldots, \delta \boldsymbol{P}_n^t]^t$ and $\delta \boldsymbol{P}_i \in R^{3\times 1}$ is the position vector from $\boldsymbol{P}_{CFi}$ on the surface of each finger link to $\boldsymbol{P}_{CBi}$ on the surface of object. The relationship between $\boldsymbol{f}_c$ and $\delta \boldsymbol{P}$ can be expressed as follows,

$$\boldsymbol{f}_c = -\boldsymbol{K}_P \delta \boldsymbol{P}. \tag{4.22}$$

The relationship between the angular displacement $\delta \boldsymbol{\theta}_s$ and the actuator torque $\boldsymbol{\tau}_s$ can be expressed as eq.(4.23).

$$\boldsymbol{\tau}_s = \boldsymbol{\tau}_{bias} - \boldsymbol{K}_\theta \delta \boldsymbol{\theta}_s \tag{4.23}$$

Substituting eqs.(4.21) and (4.22) into eq.(4.5), we have the relationship among $\delta \boldsymbol{\theta}_s$, $\delta \boldsymbol{x}$ and $\boldsymbol{W}_{ext}$ as follows,

$$\boldsymbol{W}_{ext} = -\{\boldsymbol{G}^t \boldsymbol{K}_P \boldsymbol{J} \delta \boldsymbol{\theta}_s - \boldsymbol{G}^t \boldsymbol{K}_P \boldsymbol{G} \delta \boldsymbol{x}\}. \tag{4.24}$$

Substituting eqs.(4.18), (4.21) and (4.22) into eq.(4.23), we also have the relationship between the displacement $\delta \boldsymbol{\theta}_s$ and $\delta \boldsymbol{x}$ as follows,

$$\delta \boldsymbol{\theta}_s = \boldsymbol{K}_{\theta e}^{-1}(\boldsymbol{\tau}_{bias} + \boldsymbol{J}^t \boldsymbol{K}_P \boldsymbol{G} \delta \boldsymbol{x}), \tag{4.25}$$

where $\boldsymbol{K}_{\theta e} = \boldsymbol{K}_{\theta} + \boldsymbol{J}^t \boldsymbol{K}_P \boldsymbol{J}$ denotes the combined stiffness matrix which is composed of both the stiffness $\boldsymbol{K}_{\theta}$ at the compliant controlled joint and the joint stiffness $\boldsymbol{J}^t \boldsymbol{K}_P \boldsymbol{J}$. The stiffness $\boldsymbol{K}_P$ and $\boldsymbol{K}_{\theta}$ is coupled in parallel when we view from the point $\boldsymbol{P}_{CFi}$. From eqs.(4.24) and (4.25), we have the following relationship between $\boldsymbol{W}_{ext}$ and $\delta \boldsymbol{x}$,

$$\boldsymbol{W}_{ext} = -\boldsymbol{G}^t \{ -\boldsymbol{K}_{Pe} \boldsymbol{G} \delta \boldsymbol{x} + \boldsymbol{K}_P \boldsymbol{J} \boldsymbol{K}_{\theta e}^{-1} \boldsymbol{\tau}_{bias} \}, \tag{4.26}$$

where $\boldsymbol{K}_{Pe} = \boldsymbol{K}_P \{ \boldsymbol{I} - \boldsymbol{J} (\boldsymbol{K}_{\theta} + \boldsymbol{J}^t \boldsymbol{K}_P \boldsymbol{J})^{-1} \boldsymbol{J}^t \boldsymbol{K}_P \}$ denotes the stiffness matrix with respect to $\boldsymbol{P}_{CBi}$ on the surface of object. The stiffness $\boldsymbol{K}_P$ and $\boldsymbol{K}_{\theta}$ is serially coupled when we view from the point $\boldsymbol{P}_{CBi}$. From eqs.(4.5) and (4.26) we derive the relationship between $\boldsymbol{f}_c$ and $\delta \boldsymbol{x}$ as follows,

$$\boldsymbol{f}_c = -\boldsymbol{K}_{Pe} \boldsymbol{G} \delta \boldsymbol{x} + \boldsymbol{K}_P \boldsymbol{J} \boldsymbol{K}_{\theta e}^{-1} \boldsymbol{\tau}_{bias}. \tag{4.27}$$

In eq.(4.27), if $\boldsymbol{K}_{\theta} = \boldsymbol{o}$ then $\boldsymbol{K}_{Pe} = \boldsymbol{o}$, $\boldsymbol{\tau}_{bias} = \boldsymbol{o}$, which means that $\boldsymbol{f}_c = \boldsymbol{o}$ even if we provide any displacement $\delta \boldsymbol{x}$ for the center of gravity of object. The second term in the right side of eq.(4.27) indicates the component of contact force by $\boldsymbol{\tau}_{bias}$. The displacement of the center of gravity of object can be expressed by using $\boldsymbol{W}_{ext}$ and the initial torque $\boldsymbol{\tau}_{bias}$,

$$\delta \boldsymbol{x} = (\boldsymbol{G}^t \boldsymbol{K}_{Pe} \boldsymbol{G})^{-1} (\boldsymbol{W}_{ext} + \boldsymbol{G}^t \boldsymbol{f}_{bias}), \tag{4.28}$$

where $\boldsymbol{f}_{bias} = \boldsymbol{K}_P \boldsymbol{J} \boldsymbol{K}_{\theta e}^{-1} \boldsymbol{\tau}_{bias}$. Finally, combining eqs.(4.27) and (4.28), we derive the contact force vector $\boldsymbol{f}_c$ in the following,

$$\boldsymbol{f}_c = -\boldsymbol{K}_{Pe} \boldsymbol{G} (\boldsymbol{G}^t \boldsymbol{K}_{Pe} \boldsymbol{G})^{-1} (\boldsymbol{W}_{ext} + \boldsymbol{G}^t \boldsymbol{f}_{bias}) + \boldsymbol{f}_{bias}. \tag{4.29}$$

However, it does not guarantee whether each contact force $\boldsymbol{f}_{ci}$ obtained from eq.(4.29) exists within the friction cone or not. Because eq.(4.29) does not contain any constraint with respect to the friction cone. Whether $\boldsymbol{f}_{ci}$ exists within the friction cone or not

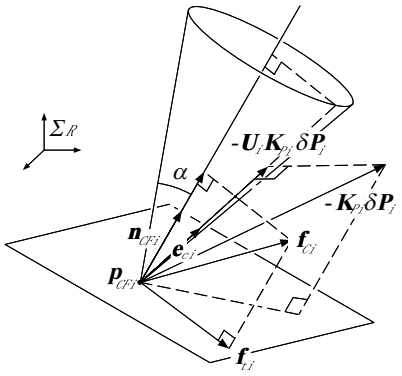

Fig. 4.4: Relationship between displacement and restoring force

can be examined by eq.(4.30),

$$\boldsymbol{n}_{CFi}^t \boldsymbol{f}_{ci} \geq \cos\alpha ||\boldsymbol{f}_{ci}||, \tag{4.30}$$

where α denotes the friction angle. Now, suppose that $\boldsymbol{f}_{ci}$ is computed outside of the friction cone as shown in Fig.4.4. Since actual $\boldsymbol{f}_{ci}$ never exists outside of the friction cone, $\boldsymbol{f}_{ci}$ as shown in Fig.4.4 implies a local slip at the contact point. This means that $\boldsymbol{f}_{ci}$ exists on the friction boundary. Based on this, we change the orientation of $\boldsymbol{f}_{ci}$ into the nearest friction boundary, where the direction $\boldsymbol{e}_{ci}$ is given by

$$\boldsymbol{e}_{ci} = \cos\alpha \boldsymbol{n}_{CFi} + \sin\alpha \frac{\boldsymbol{f}_{ti}}{||\boldsymbol{f}_{ti}||}, \tag{4.31}$$

where $\boldsymbol{f}_{ti} = \boldsymbol{f}_{ci} - (\boldsymbol{n}_{CFi}^t \boldsymbol{f}_{ci})\boldsymbol{n}_{CFi}$. For restricting the direction of restoring force $-\boldsymbol{K}_{Pi}\delta\boldsymbol{P}_i$ towards the direction of $\boldsymbol{e}_{ci}$, we introduce the linear transformation matrix $\boldsymbol{U}_i \in R^{3\times 3}$ defined by

$$\boldsymbol{U}_i = \boldsymbol{e}_{ci}\boldsymbol{e}_{ci}^t. \tag{4.32}$$

On the other hand, $\boldsymbol{U}_j = diag[1,1,1]$ when $\boldsymbol{f}_{cj}$ exists within the friction cone. From eq.(4.22), we can obtain:

$$\hat{\boldsymbol{f}}_c = -\boldsymbol{U}\boldsymbol{K}_P\delta\boldsymbol{P}, \tag{4.33}$$

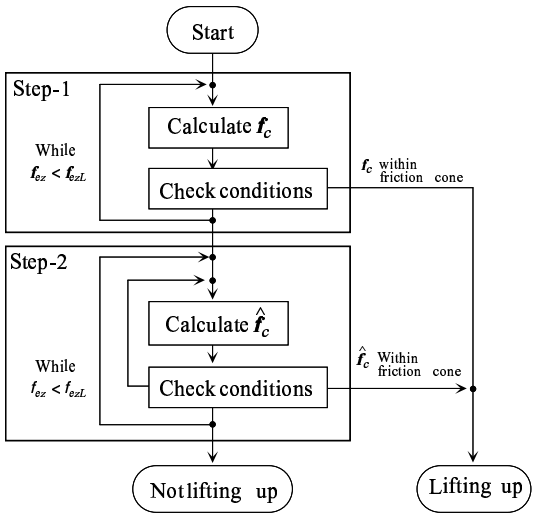

Fig. 4.5: Flow chart of the algorithm

where $\boldsymbol{U} = diag[\boldsymbol{U}_1, \ldots, \boldsymbol{U}_n] \in R^{3n \times 3n}$, and "$\hat{*}$" denotes the value when contact force is projected on the friction boundary. From eqs.(4.5) and (4.18), we obtain

$$\boldsymbol{W}_{ext} = -\boldsymbol{G}^t \hat{\boldsymbol{f}}_c, \tag{4.34}$$

$$\boldsymbol{\tau}_s = \boldsymbol{J}^t \hat{\boldsymbol{f}}_c. \tag{4.35}$$

From eqs.(4.21), (4.23), (4.33), (4.34) and (4.35), the contact force vector $\hat{\boldsymbol{f}}_c$ can be obtained as follows,

$$\hat{\boldsymbol{f}}_c = -\hat{\boldsymbol{K}}_{Pe}\boldsymbol{G}(\boldsymbol{G}^t\hat{\boldsymbol{K}}_{Pe}\boldsymbol{G})^{-1}(\boldsymbol{W}_{ext} + \boldsymbol{G}^t\hat{\boldsymbol{f}}_{bias}) + \hat{\boldsymbol{f}}_{bias}, \tag{4.36}$$

where $\hat{\boldsymbol{K}}_{Pe} = \boldsymbol{U}\boldsymbol{K}_P(\boldsymbol{I} - \boldsymbol{J}\hat{\boldsymbol{K}}_{\theta e}^{-1}\boldsymbol{J}^t\boldsymbol{U}\boldsymbol{K}_P)$, $\hat{\boldsymbol{K}}_{\theta e} = \boldsymbol{K}_\theta + \boldsymbol{J}^t\boldsymbol{U}\boldsymbol{K}_P\boldsymbol{J}$, and $\hat{\boldsymbol{f}}_{bias} = \boldsymbol{U}\boldsymbol{K}_P\boldsymbol{J}\hat{\boldsymbol{K}}_{\theta e}^{-1}\boldsymbol{\tau}_{bias}$.

By using these equations, we explain the procedure to judge whether the robot hand can lift up the object by utilizing $SPCM\{\boldsymbol{K}_\theta, \Delta\boldsymbol{\theta}_p\}$ or not. Fig.4.5 shows the flow chart diagram for explaining the procedure. Suppose that the upper limit of the virtual external force f_{ez} is f_{ezL}. The procedure can be separated into the following two steps:

Step-1 Compute $\boldsymbol{f}_c$ by using eq.(4.29) from $f_{ez} = 0$ to $f_{ez} \leq f_{ezL}$. For the computed $\boldsymbol{f}_c$, examine whether all contact force $\boldsymbol{f}_{ci}(i = 1, \ldots, n)$ satisfy ineq.(4.30) or not. If this is the case, the robot hand can lift up the object. If this is not the case, go to Step-2.

Step-2 Examine which contact force does not satisfy ineq.(4.30). Obtain the transformation matrix $\boldsymbol{U}_i$ based on eq.(4.32). Compute $\hat{\boldsymbol{f}}_c$ by using eq.(4.36). Examine whether $\hat{\boldsymbol{f}}_c$ satisfies ineq.(4.30) or not. If this is the case, the robot hand can lift up the object.

4.2.4 Simulation

Fig.4.6 shows a simulation model where the robot hand consists of three same fingers and each finger has three links. Each finger consists of the compliant controlled, locked and position–controlled joint, where the lengths of each link are $40[mm]$, $25[mm]$ and $25[mm]$, respectively, and the diameter of fingertip is $D_{tip} = 10[mm](R = 5[mm])$. The object is the cylinder whose mass is $m_B = 0.04[kg]$ and the diameter is $\phi 20[mm]$. The friction angle between the surface of object and the link is changed as a parameter. Figs.4.7(a) and (b) show the k_θ–$\Delta\theta_p$ map where $k_{\theta 1} = k_\theta$, $k_{\theta 2} = k_{\theta 3} = k_\theta/2$ and $\Delta\theta_{p1} = \Delta\theta_{p2} = \Delta\theta_{p3} = \Delta\theta_p$. When we choose the combination of $\Delta\theta_p$ and k_θ within the hatched region whose boundary is given by a thick line, it is guaranteed that the robot hand can lift up the object from the table, as far as the contact force appears within the friction cone. The region provides us with a sufficient condition, while it may be a bit strict condition. The thin lines are calculated by using the CSM (Contact Stiffness Model) under the contact stiffness $\boldsymbol{K}_{Pi} = diag[100, 100, 100]$ $([N/mm])$ for five different friction angles of $\alpha = 0.01[deg]$, $5[deg]$, $15[deg]$ and $30[deg]$. It should be noted that the result under the contact stiffness model always provides us with a mild

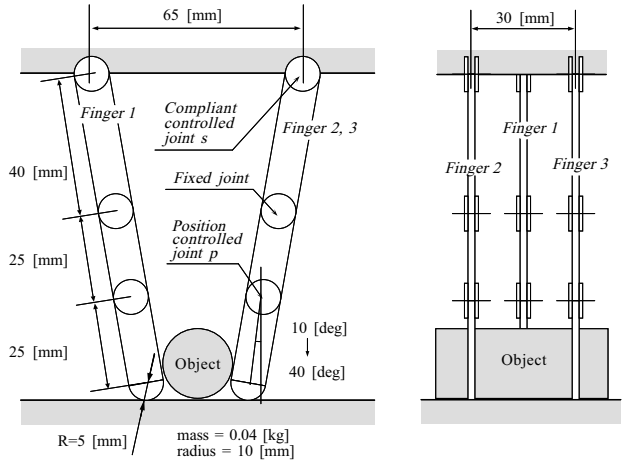

Fig. 4.6: Simulation model

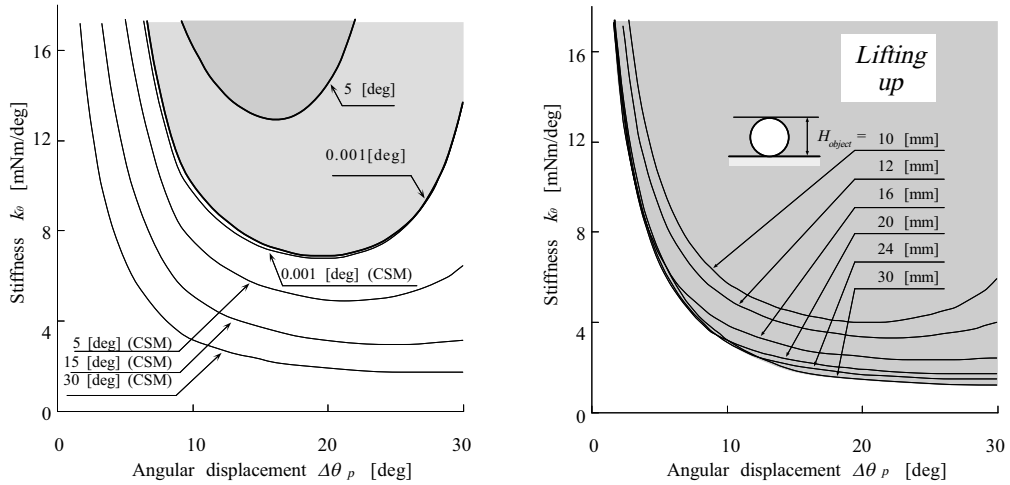

(a) Relationship with friction angle

(b) Relationship with size of object

Fig. 4.7: Simulation results

condition, namely the thin line is always lower than that of the sufficient condition obtained along the procedure explain in subsection 4.2.2. It should be also noted that both thick and thin lines eventually converge to be a single one as $\alpha \to 0$, which guarantees the validity of the simulation. During such a lifting phase, either rolling or sliding motion or a combined motion may occur. We do not care what kind of motion actually happens but have interest only whether the object is lifted up or not.

Fig.4.7(b) shows simulation results for various sizes ($H_{object} = 10, 12, 16, 20, 24, 30[mm]$) of objects where the mass and the friction angle of object are $0.04[kg]$ and $5[deg]$, respectively. As the size of object increases, the region guaranteeing that the robot hand can lift up the object from the table becomes large. From Fig.4.7(b), we can find a guideline for choosing k_θ and $\Delta\theta_p$. Roughly speaking, they should be chosen from the area computed for a small H_{object}, since the area includes other areas computed for larger objects.

4.3 Experimental Approach

Fig.4.8 shows a series of finger postures during a *DAM* by the robot hand, where the first, the second and the third joints are assigned as compliant, locked, and position–controlled joint, respectively. As each position–controlled joint rotates from $15[deg]$ to $80[deg]$, the robot hand lifts up the object from the table (*Rolling–up phase*) as shown in Fig.4.8(b). Finally, the contact condition between the finger link and the object results in sliding contact (*Wedge–effect phase*) as shown in Fig.4.8(c). After every fingertip link rotates $80[deg]$, the constant torque control is applied for achieving an enveloping grasp as shown in Fig.4.8(d).

We also examined the condition for lifting up the object by changing the combination between k_θ and $\Delta\theta_p$. Fig.4.9 shows experimental results, where $\times$, $\triangle$, and $\bigcirc$ denote failure in *DAM*, failure in *DAM* but success in lifting the object, and completely success in *DAM*, respectively. For comparison purpose, Fig.4.9 also includes simulation results where the thin line and the thick line are the lower boundaries given by the sufficient condition and by the contact stiffness model (CSM), respectively. Under a large contact friction $\alpha = 30[deg]$, the sufficient condition discussed in subsection 4.2.2 does not

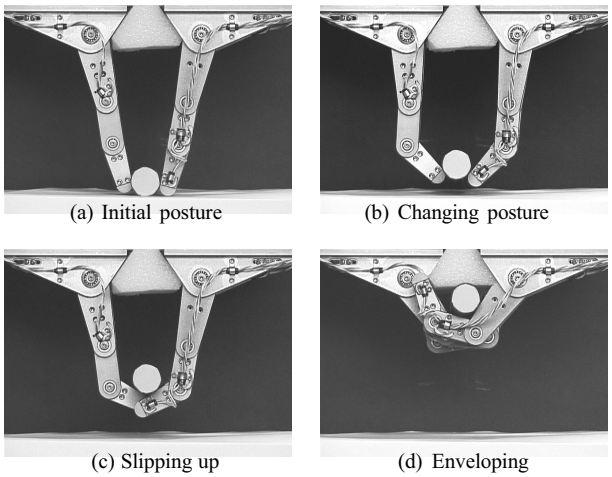

Fig. 4.8: Experimental results by robot hand

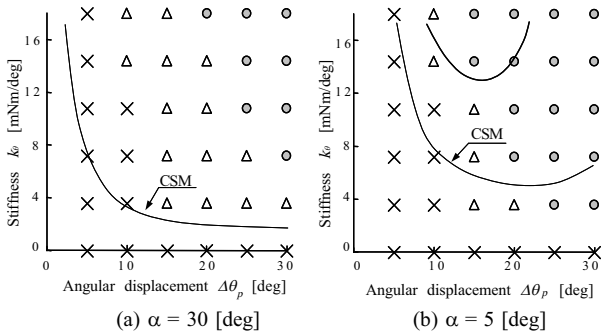

Fig. 4.9: Experimental results (k_θ–$\Delta\theta_p$ map)

provide any solution, while we can still find a large area where the robot hand is able to lift up the object. Under a small contact friction $\alpha = 5[deg]$, we can find a small area providing the sufficient condition, while the solution based on the contact stiffness model supplies a large area where $\boldsymbol{K}_{Pi} = diag[100, 100, 100]$ $([N/mm])$ is given. Overall, we can see the nice coincidence between simulation and experiments in qualitatively. Furthermore, it should be noted that the results based on the contact stiffness model are closely matching with experimental results when the contact stiffness is chosen properly.

4.4 Detecting Contact Stiffness of Object

The assumption A1-7 means that the object is stiff enough. However, not all objects in ordinary environments are stiff enough – there are many objects that are as compliant as rubber balls. In general, knowing the contact stiffness of such a compliant object is important for the robot hand to set an adequate grasping force appropriate to the compliance of the object. Moreover, suppose that the robot hand applies the *DAM* for such object. We have proposed two models in subsection 4.2.2 and 4.2.3. In the compliant contact model, deformation of object at each contact point is considered, while the rigid contact model does not. By detecting the local stiffness of object, we can obtain more appropriate stiffness of each compliant controlled joint by using the contact stiffness model.

There are several works that deal with the problem of determining the optimum grasping force considering the compliance of objects. However, the compliance of objects has been modeled as one–dimensional spring in most works[48]-[51]. On the other hand, we assume that an object consists of bundled multiple one–dimensional springs. Such an object can be represented by a stiffness matrix including the coupling components. In general, the stiffness of an object can be sensed only through the active sensing based on tactile sensors as shown in Fig.4.10. However, applying a force may result in a significant deformation of the object and making its shape significantly different from the original shape when the contact stiffness is low. It is generally difficult to estimate the initial contact point $\boldsymbol{p}_{ci}$ directly using sensor information at the instant when the hand and the object come into contact, as it involves the problem of collision. However, using torque sensor outputs, it is relatively easy to estimate, the point $\boldsymbol{p}^*_{ci}$ where the hand and the object have reached equilibrium. Considering the above facts,

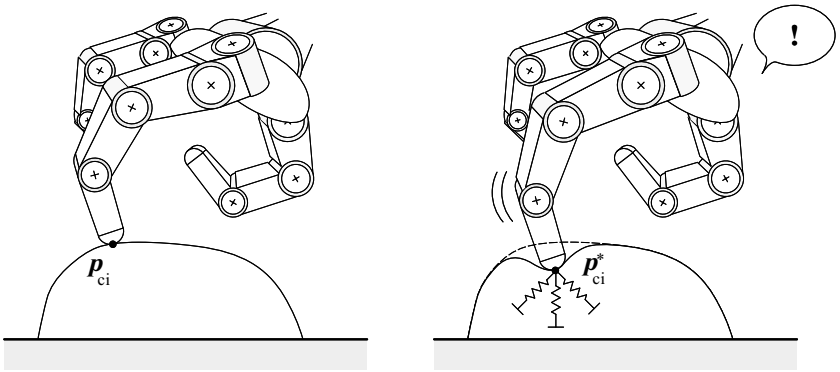

(a) Initial contact point (b) Equilibrium point

Fig. 4.10: An overview of a finger sensing.

we discuss the process of estimating the point $\boldsymbol{p}^*_{ci}$, where equilibrium has been reached, and then estimating the contact stiffness of object.

Now, we impose additionally three assumptions as follows:

(A4-1) The contact stiffness of object is limited to the linear range.

(A4-2) The object can deform, but the whole object does not move through sliding.

(A4-3) The robot hand is provided with sufficient degrees of freedom (at least 3DOF) to localize the fingertip at any point in three–dimensional space.

Let us assume that the robot is in the initial state shown in Fig.4.11(a). Let $\boldsymbol{p}^*_{ci} = [p^*_{cix}, p^*_{ciy}, 0]^t$ be the point of contact in this state, and let $\boldsymbol{p}_{ci}$ be the point where the robot first comes in contact with the object. Let τ^*_{i1} and τ^*_{i2} denote the torques of the joints in the equilibrium state. If the distance between the second joint and the contact point is represented by l^*, then the relationship between the torques and the contact force in the direction of the normal f_n represented by eqs.(4.37) and (4.38) holds.

$$\tau^*_{i1} = (l_1 + l^*) f_n \tag{4.37}$$

$$\tau^*_{i2} = l^* f_n \tag{4.38}$$

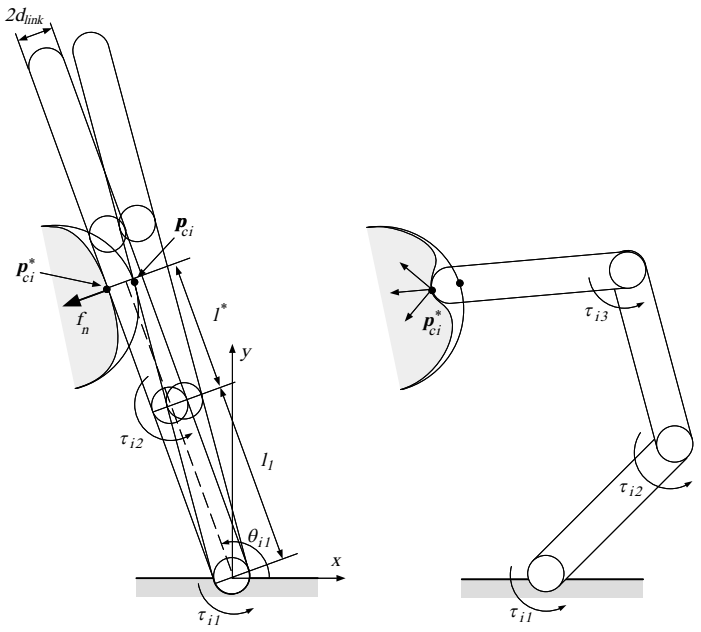

(a) Equilibrium point sensing (b) Push-in motion

Fig. 4.11: Active sensing motion.

Contact force is caused by frictional force f_t in addition to f_n. However, it should be noted that f_t has no influence on the joint torque unless the contact point is extremely close to the joint. The point $\boldsymbol{p}^*_{ci}$ on the $x-y$ plane can be approximately given by eqs.(4.39) and (4.40) unless the contact point is extremely close to the joint.

$$p^*_{cix} = l_1 \cos\theta^*_{i1} + \sqrt{l^{*2} + d^2_{link}}\cos(\theta^*_{i1} + \tan^{-1}\frac{d_{link}}{l^*}) \quad (4.39)$$

$$p^*_{ciy} = l_1 \sin\theta^*_{i1} + \sqrt{l^{*2} + d^2_{link}}\sin(\theta^*_{i1} + \tan^{-1}\frac{d_{link}}{l^*}) \quad (4.40)$$

where d_{link} represents half of the link width. If the object is stiff, the initial contact point can be easily found using eqs.(4.39) and (4.40). However, if the object is compliant, this point does not always coincide with the initial contact point $\boldsymbol{p}_{ci}$.

In general, sensing the stiffness of an object requires at least the application of a force to the object with active motion and the observation of the change in the contact force and the displacement. However, applying a force to the object with the inner side of

the link produces the problem that the contact area suddenly changes, which makes it difficult to detect the stiffness of the object accurately. Hence, we employ a method in which the stiffness of the object is sensed by using the fingertip as shown in Fig.4.11(b). This can be done by shifting the fingertip to the equilibrium point immediately when an equilibrium point is obtained.

The fingertip is moved from the equilibrium point $\boldsymbol{p}_{ci}^{*}$ by an infinitesimal displacement vector $\Delta\boldsymbol{p}_{ci} \in R^{3\times 1}$. The relationship between the contact force infinitesimal displacement vectors $\Delta\boldsymbol{f}_{ci} \in R^{3\times 1}$ and $\Delta\boldsymbol{p}_{ci}$ can be expressed by eq.(4.41) using a stiffness matrix $\boldsymbol{K}_{Pi} \in R^{3\times 3}$.

$$\Delta\boldsymbol{f}_{ci} = \boldsymbol{K}_{Pi}\Delta\boldsymbol{p}_{ci}. \tag{4.41}$$

It should be noted that, in stiffness sensing, a three–dimensional push–in motion is assumed instead of a constraint plane. The relationship between $\Delta\boldsymbol{f}_{ci}$ and the infinitesimal displacement in the joint torque $\Delta\boldsymbol{\tau}_i = [\Delta\tau_{i1}, \Delta\tau_{i2}, \Delta\tau_{i3}]^t$ is expressed by eq.(4.42).

$$\Delta\boldsymbol{\tau}_i = \boldsymbol{J}^t\Delta\boldsymbol{f}_{ci} \tag{4.42}$$

Eq.(4.42) enables us to estimate the contact force of the fingertip from the outputs of the joints' torque sensors. Actually, $\boldsymbol{J}$ can not be determined unless the exact position of the contact point of the fingertip is known. Assuming that the effect of the change of $\boldsymbol{J}$ on the estimated stiffness is considered very small, we can determine $\boldsymbol{J}$ using the link length of a representative point of the fingertip. The relationship between infinitesimal joint displacement vector $\Delta\boldsymbol{\theta}_i = [\Delta\theta_{i1}, \Delta\theta_{i2}, \Delta\theta_{i3}]^t$ and $\Delta\boldsymbol{p}_{ci}$ is expressed by eq.(4.43).

$$\Delta\boldsymbol{p}_{ci} = \boldsymbol{J}\Delta\boldsymbol{\theta}_i \tag{4.43}$$

Hence, infinitesimal displacement and fingertip force can be estimated from joint torque and joint angles using eqs.(4.42) and (4.43).

Sensing the stiffness is equivalent to determining the nine parameters in $\boldsymbol{K}_{Pi}$. The equations obtained as a result of the k-th push–in motion are as follows:

$$\Delta f_{cix}^{(k)} = k_{ixx}\Delta p_{cix}^{(k)} + k_{ixy}\Delta p_{ciy}^{(k)} + k_{ixz}\Delta p_{ciz}^{(k)} \tag{4.44}$$

$$\Delta f_{ciy}^{(k)} = k_{iyx}\Delta p_{cix}^{(k)} + k_{iyy}\Delta p_{ciy}^{(k)} + k_{iyz}\Delta p_{ciz}^{(k)} \tag{4.45}$$

$$\Delta f_{ciz}^{(k)} = k_{izx}\Delta p_{cix}^{(k)} + k_{izy}\Delta p_{ciy}^{(k)} + k_{izz}\Delta p_{ciz}^{(k)} \tag{4.46}$$

where the superscript (k) denotes that the equation corresponds to the k-th push–in motion. The above relationship indicates that three independent equations are obtained as a result of one sensing motion. Consequently, the determination of all components of a stiffness matrix requires at least three push–in motions in different directions. We determine every component of the stiffness matrix by means of the least squares method through several ($r \geq 3$) push–in motions.

$$\boldsymbol{F}_{ci} = \boldsymbol{A}_k \boldsymbol{K}_{Psi} \tag{4.47}$$

where $\boldsymbol{K}_{Psi} = [k_{ixx}, k_{ixy}, k_{ixz}, \ldots, k_{izz}]^t$, $\boldsymbol{F}_{ci} = [\Delta f_{cix}^{(1)}, \Delta f_{ciy}^{(1)}, \Delta f_{ciz}^{(1)}, \ldots, \Delta f_{ciz}^{(r)}]^t$, and $\boldsymbol{A}_k \in R^{3r\times 9}$ represents coefficient matrix. Finally, every element of the stiffness matrix is obtained by eq.(4.48).

$$\boldsymbol{K}_{Psi} = [\boldsymbol{A}_k^t \boldsymbol{A}_k]^{-1} \boldsymbol{A}_k^t \boldsymbol{F}_{ci} \tag{4.48}$$

Fig.4.12 shows a simulation result for a three–fingered robot hand, where each finger has three joints. Each finger consists of the compliant controlled, locked and position–controlled joint, respectively. The friction angle α between the surface of object and link is $5[deg]$. The thin lines and the thick lines are obtained under the contact stiffness $\boldsymbol{K}_{Pi} = k_P\ diag[1,1,1]$ where $k_P = 10, 1, 0.5, 0.1[N/mm]$ and

$$\boldsymbol{K}_{Pi} = k_P \begin{bmatrix} 1 & 0.5 & 0.8 \\ 0.5 & 1 & 0.5 \\ 0.8 & 0.5 & 1 \end{bmatrix}$$

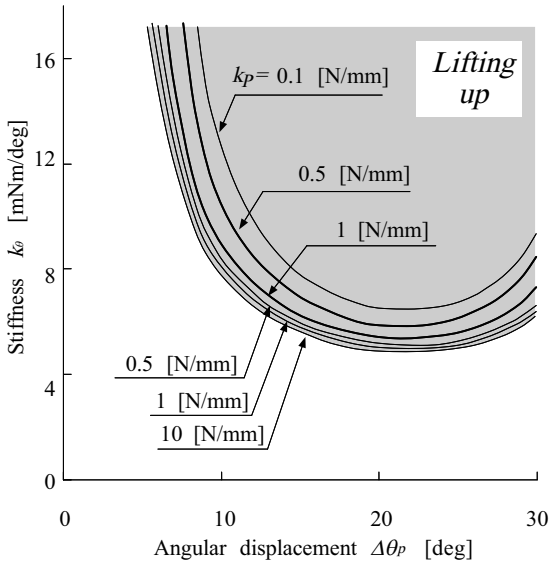

Fig. 4.12: Simulation result of DAM with various k_p

where $k_P = 1, 0.5[N/mm]$, respectively. The region where the robot hand can lift up the object changes according to $\boldsymbol{K}_{Pi}$. In addition to the shape and the mass of object, if the contact stiffness can be obtained, we can design the appropriate joint compliance with respect to $\Delta\theta_{pi}$ by using Fig.4.12.

4.5 Summary

Taking note that the *self–posture changing motion* can well simulate the *DAM*, we considered the condition for lifting up the object. We introduced a sufficient condition, through it is quite conservative. We also explored the lifting–up condition by assuming that there exists contact stiffness at each contact point. It should be noted that both approaches have a nice coincidence under an extremely small contact friction. We also implemented the *SPCM* into the grasp procedure of a multi–fingered robot hand and verified its effectiveness experimentally. Furthermore, we have discussed an approach for detecting the local stiffness of the object by utilizing active sensing.

Chapter 5

Grasp Strategy Simplified by DAM

5.1 Introduction

Figs.5.1(a) and (b) show the results of grasping experiment where the objects are covered by either a drawing paper or a rubber, respectively, so that we can change the surface friction. The horizontal axis and the vertical axis denote the shape of object and the normalized value $d_{obj} = H_{object}/D_{tip}$, respectively, where H_{object} and D_{tip} denote the height of object and the diameter of fingertip, respectively. $d_{obj} = 1.0$ means that the height of object and the diameter of fingertip are same. As the height of object increases, d_{obj} also becomes larger. We prepare four types of objects where the cross–section shape of objects are circle, hexagon, rectangle and triangle, respectively. "$\bigcirc$" and "$\times$" denote the results of grasp experiment where the robot hand can successfully grasp the object and fail in grasping, respectively. The robot hand can grasp the following objects; a circular object whose d_{obj} is larger than 0.7, a hexagonal object whose d_{obj} is larger than 0.9, and a rectangular object whose d_{obj} is larger than 1.2. Although the robot hand can grasp the rectangular object, the motion is quite unstable due to the existence of the edge. The triangular object with small contact friction can not be lifted up from the table in *Rolling–up phase*. The robot hand can not achieve

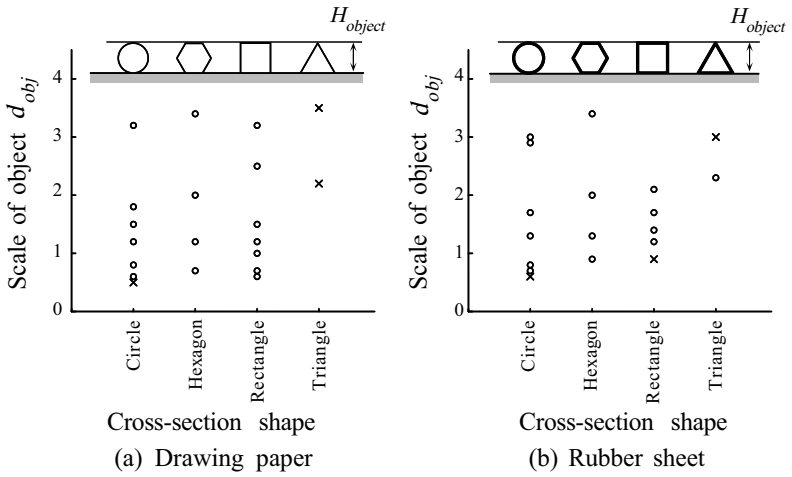

Fig. 5.1: Experimental results for various column objects

the enveloping grasp for a triangular object under large contact friction, even if it can be lifted up from the table. For triangular objects, the grasp system often becomes unstable when the edge part makes contact with the link after lifting up. This behavior is similar to the grasped coin instability where the grasped coin by fingertips results in collapse when we increase the internal force.

The most interesting aspect of this experiment is that the *DAM* can be applied not only to small objects but also to comparatively large objects, for example, a circular object whose $d_{obj} = 3.0$. In section 2.3, we applied the grasping strategy incorporating the *wedge–effect* for achieving the enveloping grasp. However, these objects can be grasped by using the *DAM*. Furthermore, the *DAM* can be applied for rectangular objects where the robot hand can not achieve the enveloping grasp by utilizing the *wedge–effect*. In spite of its simple grasping motion, the *DAM* has a potential application field for detaching the objects of various sizes, shapes and contact friction.

In this chapter, by focusing on the advantage of *DAM* (or *SPCM*), we challenge to construct a *generalized grasp strategy (GGS)* which is applicable not only for small

sized objects but also for other sized objects.

5.2 Generalized Grasp Strategy (GGS)

Fig.5.2 shows an example of *GGS* where it includes the *DAM* (or *SPCM*) in the central part. Now, let us assume that the robot hand has a vision sensor. From the vision information, the robot can recognize the size of object. In case that the object is large enough ($1.0 < d_{robot}$) to grasp it directly, the robot chooses the *direct grasp* which is given by subsection 2.3.4. In case that the object is small ($d_{robot} \leq 1.0$), the robot chooses the grasp strategy with *DAM*. When the robot recognizes that the *initial adjustment motion* is necessary, the robot includes the *initial adjustment motion* as shown in Fig.5.3.

Depending upon the contact friction, the object may stop due to so called jamming during the *DAM*. When such a failure is detected, one feasible approach to recover is to apply small vibration signal (dither signal) to each joint, so that we can reduce the equivalent contact friction[47].

5.3 Experimental Results

Figs.5.4(a), (b) and (c) show series of finger postures during the *GGS* by the robot hand for a large, a middle sized and a small object, respectively. For a large object, the robot hand achieves the enveloping grasp by utilizing the *direct grasp*. For a middle–sized object and a small object, the robot hand achieves the enveloping grasp by utilizing the *DAM*.

Figs.5.5(a) and (b) show the experimental results where objects used in Figs.5.5(a) and

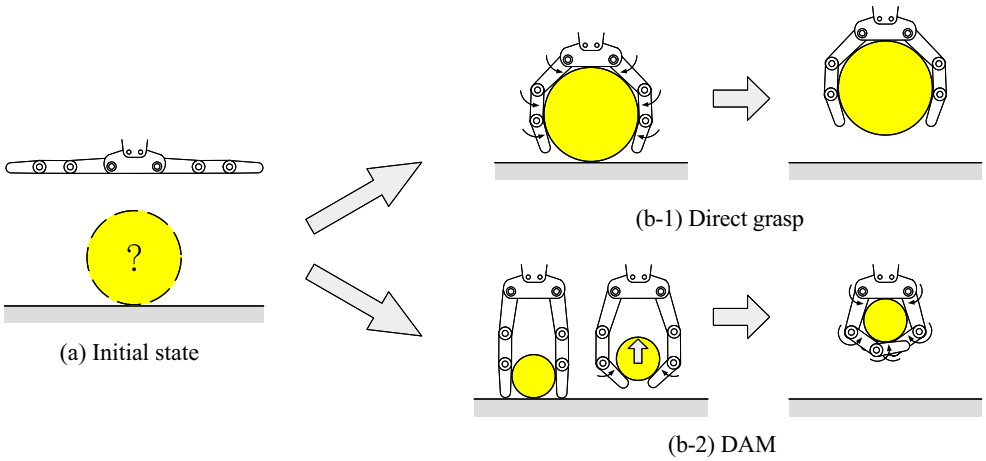

Fig. 5.2: Generalized Grasp Strategy (GGS)

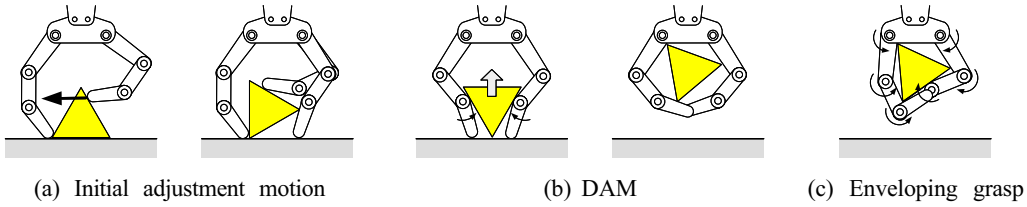

Fig. 5.3: DAM with initial adjustment motion

(b) are covered by drawing paper and by rubber, respectively. The horizontal and the vertical axes denote the shape of object and the normalized value $d_{robot} = L_o/L_r (L_r = 224[mm])$, respectively, where L_o and L_r denote the circumference of the object and the distance between fingertips, respectively. As the height of object increases, d_{robot} also increases. We prepare four types of object where cross–section shapes of object are circle, hexagon, rectangle and triangle, respectively. "◯" and "•" denote that the robot hand can be achieved the enveloping grasp by utilizing the *GGS* and by utilizing the *GGS* with *initial adjustment motion*, respectively. The experimental results show that the robot hand can grasp various kinds of objects by utilizing the *GGS* proposed here.

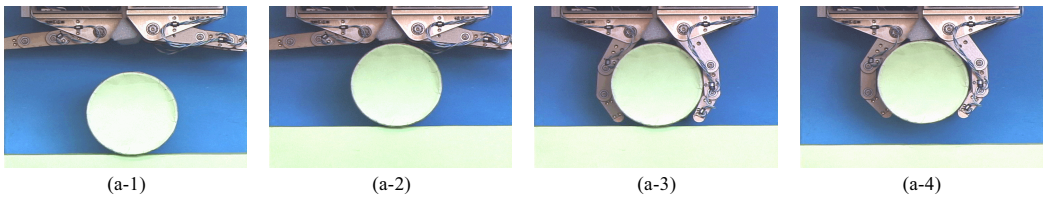

(a-1) (a-2) (a-3) (a-4)

(a) Large object (d_{robot} = 1.1)

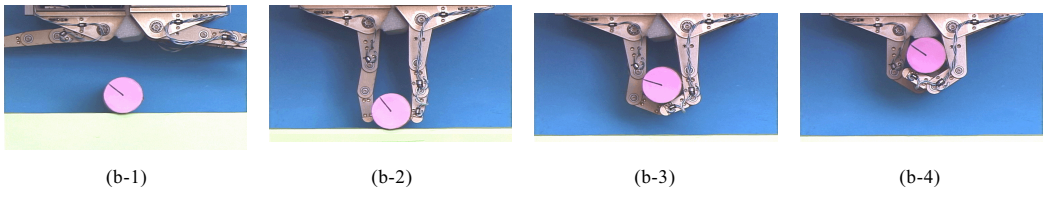

(b-1) (b-2) (b-3) (b-4)

(b) Middle sized object (d_{robot} = 0.4)

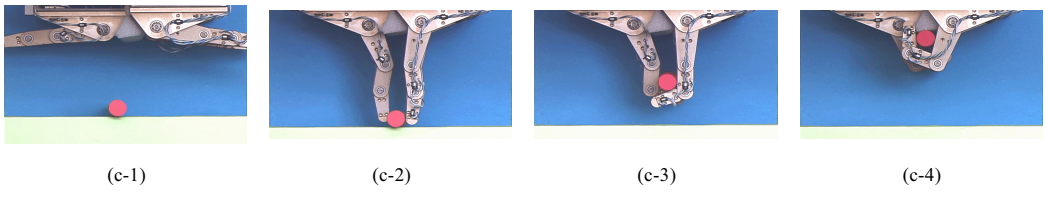

(c-1) (c-2) (c-3) (c-4)

(c) Small object (d_{robot} = 0.2)

Fig. 5.4: Experimental results of GGS

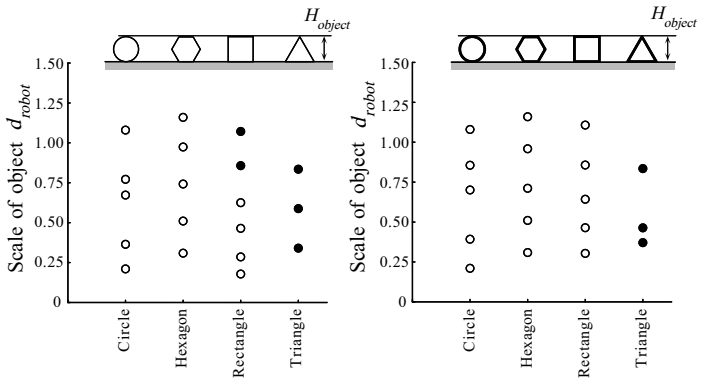

(a) Drawing paper (b) Rubber sheet

Fig. 5.5: Experimental results for general column objects.

5.4 Summary

We have shown that the *DAM* can be applied for cylindrical objects with various sizes, shapes and contact friction. Based on the advantage of *DAM*, we have proposed new

grasping strategy, the *GGS*. We have experimentally shown that the robot hand can achieve the enveloping grasp for most kinds of objects with various sizes, cross–section shapes, and contact friction by utilizing the *GGS*.

Chapter 6

Conclusions

In this dissertation, we have discussed how to implement human motion planning into a multi–fingered robot hand. In order to solve this problem, we have observed the human motion for grasping column objects placed on a table. Through the experiment, we have discovered several interesting human behaviors. We have analyzed these human behaviors in detail, and also transferred them into a multi–fingered robot hand.

In chapter 1, we have explained the background of this work and related works.

In chapter 2, through the observation of humans, we have found that humans unconsciously change the grasp strategy according to the size, cross–section shape, and contact friction of the objects. We have called this grasp planning the *Scale–Dependent Grasp*. We have roughly separated the grasping procedures into the three tasks so that we could construct grasping strategies easily applicable to multi–fingered robot hands. Based upon this interpretation of human grasping motion, we have proposed five basic grasping strategies. For choosing an appropriate strategy according to the size, friction and geometry of an object, we have introduced a *guide–line–map*. We have discussed the strategy flow diagram to explain how to switch from one grasping strategy to another when the robot hand fails to grasp an object. We have also relaxed the

assumptions, so that we can apply the grasping strategies to general objects.

In chapter 3, we have focused on a small object whose representative size is smaller than that of our fingertips. Through the observation of human grasping motion, we have discovered the *Detaching Assist Motion (DAM)*. We have analyzed the change of finger posture during the *DAM* and explained the basic working mechanism of *DAM*.

In chapter 4, we have implemented the *DAM* for the multi–fingered robot hand by utilizing the *Self–Posture Changing Motion (SPCM)* which is easily implemented by robot hands. We have examined the conditions leading to the *DAM* by using *SPCM*. As for the condition for lifting an object, we have explored a sufficient condition and compared it with contact stiffness model. We have implemented the *SPCM* into the grasp procedure of a multi–fingered robot hand and verified its effectiveness experimentally. Experimental results have proved to be comparable to simulation results. We have discussed an approach for detecting the local stiffness of the object where the finger makes contact. Supposing that the robot hand applies the *DAM*, by detecting the local stiffness of object we can obtain more appropriate stiffness of each compliant controlled joint by using the contact stiffness model.

In chapter 5, we have made it clear that the *DAM* can be applied not only to small objects but also to relatively large objects experimentally. By considering this advantage of *DAM*, we have proposed new grasping strategy, the *Generalized Grasp Strategy (GGS)*. We have experimentally confirmed that the multi–fingered robot hand can achieve the enveloping grasp for various kinds of objects by using the *GGS*.

In this dissertation, we have supposed that the shape of the object is a cylinder. Extension of the object's shape from a cylinder to a general three-dimensional shape will improve the utility of this work. Although we have focused on how to achieve the en-

veloping grasp for an object placed on a table, we believe that the property employed in this work will be able to apply for another usual human motion in daily life.

Finally, publications concerning in this dissertation are listed in the bibliography [52]–[57].

Bibliography

[1] G. Hizinger: "The Space and Telerobotic Concepts of DFVLR ROTEX," *Proceedings of the IEEE International Conference on Robotics and Automation*, Vol.1, pp. 443-449, 1987.

[2] H.A. Ernst: "MH–1, *A Computer–Operated Mechanical Hand," Theoretical Problems in Artificial Intelligence*, pp. 39-51, 1971.

[3] T. Okada: "Object–Handling System for Manual Industry," *IEEE Transactions on Systems, Man, and Cybernetics*, Vol. 9, No. 2, pp. 79–86, 1979.

[4] J.K. Salisbury and J.J. Craig: "Articulated Hands (Force Control and Kinematics Issues)," *International Journal of Robotics Research*, Vol. 1, No. 1, pp. 4–20, 1982.

[5] S.C. Jacobsen et al. : "Design of the Utah/MIT Dexterous Hand," *Proceedings of the IEEE International Conference on Robotics and Automation*, pp. 1520–1528. 1986.

[6] M. Cutkosky: "On Grasp Choice, Grasp Models, and the Design of Hands for Manufacturing Tasks," *IEEE Transactions on Robotics and Automation*, Vol. 5, No. 3, JUNE, pp. 269–279, 1989.

[7] G.A. Bekey, H. Liu, R. Tomovic, and W. Karplus: "Knowledge-based Control of Grasping in Robot Hands Using Heuristics from Human Motor Skills," *IEEE*

Transactions on Robotics and Automation, Vol. 9, No. 6, DECEMBER, pp. 709–722, 1993.

[8] S.B. Kang and K. Ikeuchi: "Toward Automatic Robot Instruction from Perception — Recognizing a Grasp from Observation," *IEEE Transactions on Robotics and Automation*, Vol. 9, No. 4, AUGUST, pp. 432–443, 1993.

[9] S.B. Kang and K. Ikeuchi: "Toward Automatic Robot Instruction from Perception – Temporal Segmentation of Tasks from Human Hand Motion," *IEEE Transactions on Robotics and Automation*, Vol. 11, No. 5, OCTOBER, pp. 670–681, 1995.

[10] F. Saito and K. Nagata: "Interpretation of Grasp and Manipulation from Functional Surfaces," *Proceedings of Robotics Symposia*, pp. 113–120, 1999, (in Japanese).

[11] Y. Kamakura, M. Matsuo, H. Ishii, F. Mitsuboshi and Y. Miura: "Pattern of static prehension in normal hands," *The American Journal of Occupational Therapy*, Vol. 34, No. 7, pp. 437-445, 1980.

[12] S. Shimizu, M. Shimojo, S. Sato, Y. Seki, A. Takahashi, Y. Inukai and M. Yoshioka: "The Relation between Human Grip Types and Force Distribution Pattern in Grasping," *Proceedings of the IEEE International Workshop on Robot and Human Communication*, pp. 286–291, 1996.

[13] M. Jeannerod: "Attention and Performance," Chapter Intersegmental Coordination during Reaching at Natural Visual Objects, pp. 153-168, Erlbaum, Hillsdale, 1981.

[14] C. Bard and J. Troccaz: "Automatic Preshaping for a Dexterous Hand from a Simple Description of Objects," *Proceedings of the IEEE International Workshop on Intelligent Robots and Systems*, pp. 865-872, 1990.

[15] M. Kaneko and K. Honkawa: "Contact Point and Force Sensing for Inner Link Based Grasps," *Proceedings of the IEEE International Conference on Robotics and Automation*, pp. 2809–2814, 1994.

[16] J.K. Salisbury: "Whole–Arm Manipulation," *Proceedings of the 4th International Symposium of Robotics Research*, Santa Cruz, CA, 1987. Published by the MIT Press, Cambridge MA.

[17] J.K. Salisbury, W. Townsend, B. Eberman, and D. Dipietro: "Preliminary Design of a Whole–Arm Manipulation System (WAMS)," *Proceedings of the IEEE International Conference on Robotics and Automation*, pp. 254, 1988.

[18] K. Mirza and D.E. Orin: "Control of Force Distribution for Power Grasp in the DIGITS System," *Proceedings of the IEEE 29th CDC Conference*, pp. 1960–1965, 1990.

[19] S. Hirose: "The Development of Soft Gripper for Versatile Robot Hand," Mechanism and Machine Theory, Pergamon Press, 13, pp. 351–359, 1978.

[20] A. Bicchi: "Force Distribution in Multiple Whole–Limb Manipulation," *Proceedings of the IEEE International Conference on Robotics and Automation*, pp. 196–201, 1993.

[21] T. Omata and K. Nagata: "Rigid Body Analysis of the Indeterminate Grasp Force in Power Grasps." *Proceedings of the IEEE International Conference on Robotics and Automation*, pp. 1787–1794, 1996.

[22] X-Y. Zhang, Y. Nakamura, K. Goda, and K. Yoshimoto: "Robustness of Power Grasp," *Proceedings of the IEEE International Conference on Robotics and Automation*, pp. 2828–2835, 1994.

[23] J.C. Trinkle, J.M. Abel, and R.P. Paul: "Enveloping, Frictionless Planar Grasping, " *Proceedings of the IEEE International Conference on Robotics and Automation*, pp. 246–251, 1987.

[24] J.C. Trinkle and R.P. Paul: "The Initial Grasp Liftability Chart," *IEEE Transactions on Robotics and Automation*, Vol. 5, No. 1, FEBRUARY, pp. 47–52, 1989.

[25] J.C. Trinkle and R.P. Paul: "Planning for Dexterous Manipulation with Sliding Contacts," *International Journal of Robotics Research*, Vol. 9, No. 3, pp. 24–48, 1990.

[26] J.C. Trinkle, R.C. Ram, A.O. Farahat, and P.F. Stiller: "Dexterous Manipulation Planning and Execution of an Enveloped Slippery Workpiece", *Proceedings of the IEEE International Conference on Robotics and Automation*, pp. 442–448, 1993.

[27] M. Kaneko, M. Higashimori, and T. Tsuji: "Transition Stability of Enveloping Grasps," *Proceedings of the IEEE International Conference on Robotics and Automation*, pp. 3040–3046, 1998.

[28] K.P. Kleinmann, J. Henning, C. Ruhm, and H. Tolle: "Object Manipulation by a Multifingered Gripper: On the Transition from Precision to Power Grasp," *Proceedings of the IEEE International Conference on Robotics and Automation*, pp. 2761–2766, 1996.

[29] N. Sarkar, X. Yun and V. Kumar: "Dynamic Control of 3–D Rolling Contacts in Two–Arm Manipulation," *IEEE Transactions on Robotics and Automation*, Vol. 13, No. 3, pp. 364–376, 1997.

[30] M. Cherif and K.K. Gupta: "Planning Quasi–static Motions for Re–configuring Objects with a Multi–fingered Robotic Hand," *Proceedings of the IEEE International Conference on Robotics and Automation*, pp. 986–991, 1997.

[31] I. Kao and M.R. Cutkosky: "Quasistatic Manipulation with Compliance and Sliding," *International Journal of Robotics Research*, Vol. 11, No. 1, pp. 20–40, 1992.

[32] A.A. Cole, P. Hsu and S.S. Sastry: "Dynamic Control of Sliding by Robot Hands for Regrasping," *IEEE Transactions on Robotics and Automation*, Vol. 8, No. 1, pp. 42–52, 1992.

[33] M.T. Mason: "Mechanics and Planning of Manipulator Pushing Operation," *International Journal of Robotics Research*, Vol. 5, No. 3, pp. 53–71, 1986.

[34] Y. Aiyama, M. Inaba and H. Inoue: "Pivoting: A New Method of Graspless Manipulation of Object by Robot Fingers," *Proceedings of the IEEE/RSJ International Conference on Intelligent Robots and Systems*, pp. 136–143, 1993.

[35] N.B. Zumel and M.A. Erdmann: "Nonprehensile Manipulation for Orientating Parts in the Plane," *Proceedings of the IEEE International Conference on Robotics and Automation*, pp. 2433–2439, 1997.

[36] K.M. Lynch: "Toppling Manipulation," *Proceedings of the IEEE International Conference on Robotics and Automation*, pp. 2551–2557, 1999.

[37] M. Kaneko, N. Thaiprasert, and T. Tsuji: "Experimental Approach on Enveloping Grasp for Column Objects," *Eds. A. Casal and A.T. de Almeida, Experimental Robotics V, the 5th International Symposium*, pp. 35–46, 1997.

[38] M. Kaneko and K. Tanie : "Contact Point Detection for Grasping an Unknown Object Using Self-Posture Changeability," *IEEE Transactions on Robotics and Automation*, Vol.10, No.3, pp.355–367, 1994.

[39] J. Kerr and B. Roth: "Analysis of Multifingered Hands," *International Journal of Robotics Research*, Vol.4, No.4, pp. 3–17, 1986.

[40] S. Hirai and H. Asada: "Kinematics and Statics of Manipulation Using the Theory of Polyhedral Convex Cones," *International Journal of Robotics Research*, Vol.12, No.5, pp. 434–447, 1993.

[41] M. Kaneko, K. Harada and T. Tsuji: "A Sufficient Condition for Manipulation of Envelope Family," *Proceedings of the IEEE International Conference on Robotics and Automation*, pp. 1060–1067, 2000.

[42] A. Bicchi: "Analysis and Control of Power Grasping," *Proceedings of IEEE/RSJ International Workshop on Intelligent Robots and Systems IROS'91*, pp. 691–697, 1991.

[43] A. Bicchi: "Force Distribution in Multiple Whole-Limb Manipulation," *Proceedings of the IEEE International Conference on Robotics and Automation*, pp. 196–201, 1993.

[44] Y. Zhang, F. Gao and W.A. Gruver: "Determination of Contact Forces in Grasping," *Proceedings of the IEEE International Conference on Intelligent Robots and Systems*, pp. 1038–1043, 1996.

[45] W. Stamps and V. Kumar: "On the Stability of Grasped Objects," *IEEE Transactions on Robotics and Automation*, Vol. 12, No. 6, DECEMBER, pp. 904–917, 1996.

[46] P. R. Kuraus, V. Kumar and P. Dupont: "Analysis of Frictional Contact Models for Dynamic Simulation," *Proceedings of the IEEE International Conference on Robotics and Automation*, pp. 9769–981, 1998.

[47] T. Shirai, M. Kaneko and T. Tsuji: "Active Friction Control of Robot Finger," *Proceedings of the 18th Annual Conference of the Robotics Society of Japan*, pp. 63–64, 2000, (in Japanese).

[48] T. Fukuda, N. Kitamura, and K. Tanie : "A Method of Robot Force Control Considering Object Characteristics (1st report)," *Transactions of Japanese Society of Mechanical Engineers*, 53–487C, pp.726, 1987, (in Japanese).

[49] T. Fukuda, T. Kitagami, and K. Tanie : "A Method of Robot Force Control Considering Object Characteristics (2nd report)," *Transactions of Japanese Society of Mechanical Engineers*, 53-496C,pp.2577, 1987, (in Japanese).

[50] Y. Shoji, T. Inaba, and T. Fukuda, "Unified Approach on Control of Robot Manipulator Including Collision," *Journal of the Robotics Society of Japan*, Vol.11, No.55, pp.55, 1993, (in Japanese).

[51] J.Kahang and F. Amirouche, "Impact Force Analysis in Mechanical Hand Design," *Journal of Robotics and Automation*, Vol.3, No.3, pp.55, 1988.

[52] T. Shirai, N. Imamura, T. Fukuda, and M. Kaneko : "Tactile Based Active Sensing for Detecting Stiffness and Contact Point Using Robotic Finger," *Journal of Robotics and Mechatronics*, Vol.8, No.6, pp. 531–537, 1996.

[53] T. Shirai, M. Kaneko and T. Tsuji: "Scale–Dependent Grasp," *Journal of the Robotics Society of Japan*, Vol .17, No. 4, pp. 111-120, 1999, (in Japanese).

[54] M. Kaneko, T. Shirai and T. Tsuji: "Scale–Dependent Grasp," *the IEEE Transaction on System, Man, and Cybernetics*, Vol. 30: Part B, No. 6, 2000, (To be published).

[55] T. Shirai, M. Kaneko, K. Harada. and T. Tsuji: "Scale–Dependent Grasps," *Proceedings of the 3rd International Conference on Advanced Mechatronics*, pp. 197–202, Okayama, Japan, August 1998, JSME.

[56] T. Shirai, M. Kaneko, K. Harada and T. Tsuji: "Enveloping Grasp with a New Detaching Strategy," *Proceedings of the 9th International Conference on Advanced Robotics*, pp. 167–172, Tokyo, Japan, Oct.25-27, 1999.

[57] M. Kaneko, T. Shirai, and T. Tsuji: "Hugging Walk," *Proceedings of the IEEE International Conference on Robotics and Automation*, pp. 2611–2616, 2000.

Acknowledgments

I wish to thank my advisor professor Makoto Kaneko for his advice, suggestions, encouragement and patience. He taught me various research fields of robotics. His serious attitude for research was an excellent example for me.

I would like to thank Professor Tsutomu Hasegawa, Professor Kouichi Harada and Professor Toshimasa Watanabe for their invaluable suggestions, discussions and comments on this dissertation.

I am very grateful to Associate Professor Toshio Tsuji for his excellent contributions, invaluable discussions and comments on this work. I also thank Research Associate, Dr. Kensuke Harada for his helpful comments and kind supports.

I would like to express my sincere gratitude for Mr. Mitushi Sawada, Mr. Kazuhiro Nakagawa and Mr. Takefumi Mukai for their helping the experiments.

I thank the friendship of Dr. Naoki Kanayama at Harmonic Drive Systems Inc., Dr. Osamu Fukuda at Mechanical Engineering Laboratory, AIST, MITI, and Ph.D student, Mr. Yoshiyuki Tanaka very much. I also thank Dr. Naohiro Ueno, the member of the Kyushu National Industrial Research Institute, AIST, MITI, for his helpful advice.

I am sure that TITAN VIII could not walk without the united efforts of Mr. Tomohiro Inoue, Mr. Noriaki Kuroda and Mr. Akihiko Mizuno.

Many thanks go to the other members of Robotics Lab. for their encouragements and supports.

Finally, I express my gratitude to my dearest wife, Nika, who had allowed and supported my selfish challenge.